Ozone and haze pollution weakens net primary productivity in China

Xu Yue[1], Nadine Unger[2], Kandice Harper[3], Xiangao Xia[4], Hong Liao[5], Tong Zhu[6], Jingfeng Xiao[7], Zhaozhong Feng[8], and Jing Li[9]

[1] Climate Change Research Center, Institute of Atmospheric Physics, Chinese Academy of Sciences, Beijing 100029, China
[2] College of Engineering, Mathematics and Physical Sciences, University of Exeter, Exeter, EX4 4QE, UK
[3] School of Forestry and Environmental Studies, Yale University, 195 Prospect Street, New Haven, Connecticut 06511, USA
[4] Laboratory for Middle Atmosphere and Global Environment Observation, Institute of Atmospheric Physics, Chinese Academy of Sciences, Beijing 100029, China
[5] School of Environmental Science and Engineering, Nanjing University of Information Science & Technology, Nanjing 210044, China
[6] State Key Laboratory for Environmental Simulation and Pollution Control, College of Environmental Sciences and Engineering, Peking University, Beijing 100871, China.
[7] Earth Systems Research Center, Institute for the Study of Earth, Oceans, and Space, University of New Hampshire, Durham, NH 03824, USA
[8] Research Center for Eco-Environmental Sciences, Chinese Academy of Sciences, Beijing 100085, China
[9] Laboratory for Climate and Ocean-Atmosphere Studies, Department of Atmospheric and Oceanic Sciences, School of Physics, Peking University, Beijing 100871, China

Corresponding author:
Xu Yue
Telephone: 86-10-82995369
Email: xuyueseas@gmail.com

Keywords: Haze pollution, climate projection, pollution mitigation, ozone damage, diffuse radiative fertilization, aerosol radiative effects, aerosol indirect effects, photosynthesis, net primary productivity

Abstract

Atmospheric pollutants have both beneficial and detrimental effects on carbon uptake by land ecosystems. Surface ozone (O_3) damages leaf photosynthesis by oxidizing plant cells, while aerosols promote carbon uptake by increasing diffuse radiation and exert additional influences through concomitant perturbations to meteorology and hydrology. China is currently the world's largest emitter of both carbon dioxide and short-lived air pollutants. The land ecosystems of China are estimated to provide a carbon sink, but it remains unclear whether air pollution acts to inhibit or promote carbon uptake. Here, we employ Earth system modeling and multiple measurement datasets to assess the separate and combined effects of anthropogenic O_3 and aerosol pollution on net primary productivity (NPP) in China. In the present day, O_3 reduces annual NPP by 0.6 Pg C (14%) with a range from 0.4 Pg C (low O_3 sensitivity) to 0.8 Pg C (high O_3 sensitivity). In contrast, aerosol direct effects increase NPP by 0.2 Pg C (5%) through the combination of diffuse radiation fertilization, reduced canopy temperatures, and reduced evaporation leading to higher soil moisture. Consequently, the net effects of O_3 and aerosols decrease NPP by 0.4 Pg C (9%) with a range from 0.2 Pg C (low O_3 sensitivity) to 0.6 Pg C (high O_3 sensitivity). However, precipitation inhibition from combined aerosol direct and indirect effects reduces annual NPP by 0.2 Pg C (4%), leading to a net air pollution suppression of 0.8 Pg C (16%) with a range from 0.6 Pg C (low O_3 sensitivity) to 1.0 Pg C (high O_3 sensitivity). Our results reveal strong dampening effects of air pollution on the land carbon uptake in China today. Following the current legislation emission scenario, this suppression will be further increased by the year 2030, mainly due to a continuing increase in surface O_3. However, the maximum technically feasible reduction scenario could drastically relieve the current level of NPP damage by 70% in 2030, offering protection of this critical ecosystem service and the mitigation of long-term global warming.

1 Introduction

Surface ozone (O_3) and atmospheric aerosols influence land ecosystem carbon uptake both directly and indirectly through Earth system interactions. O_3 reduces plant photosynthesis directly through stomatal uptake. The level of damage is dependent on both surface ozone concentrations ([O_3]) and the stomatal conductance (g_s), the latter of which is closely related to the photosynthetic rate (Reich and Amundson, 1985; Sitch et al., 2007; Ainsworth et al., 2012). The impact of aerosol pollution on vegetation is less clear. Atmospheric aerosols influence plant photosynthesis through perturbations to radiation, meteorology, and clouds. Observations (Cirino et al., 2014; Strada et al., 2015) suggest that an increase in diffuse light partitioning in response to a moderate aerosol loading can improve canopy light use efficiency (LUE) and promote photosynthesis, known as diffuse radiation fertilization (DRF), as long as the total light availability is not compromised (Kanniah et al., 2012). Atmospheric aerosols also reduce leaf temperature (Steiner and Chameides, 2005; Cirino et al., 2014), but the consequence for photosynthesis depends on the relationship between the local environmental temperature and the photosynthetic optimum temperature of approximately 25°C. Aerosol-induced changes in evaporation and precipitation are interconnected but impose opposite effects on photosynthesis; less evaporation preserves soil moisture in the short term but may decrease local rainfall (Spracklen et al., 2012) and lead to drought conditions in the long term. Furthermore, aerosol indirect effects (AIE) on cloud properties can either exacerbate or alleviate the above feedbacks.

China is currently the world's largest emitter of both carbon dioxide and short-lived air pollutants (http://gains.iiasa.ac.at/models/). The land ecosystems of China are estimated to provide a carbon sink (Piao et al., 2009), but it remains unclear how air pollution may affect this sink through the atmospheric influences on regional carbon uptake. O_3 damages to photosynthesis, including those in China, have been quantified in hundreds of measurements (Table S1), but are limited to individual plant species and specific O_3 concentrations ([O_3]). Previous regional modeling of O_3 vegetation damage (e.g., Ren et al., 2011; Tian et al., 2011) does not always take advantage of valuable observations to calibrate GPP-O_3 sensitivity coefficients for China domain and typically the derived results have not been properly validated. The aerosol effects on photosynthesis are less well understood. Most of the limited observation-based studies (Rocha et al., 2004; Cirino et al., 2014; Strada et al., 2015) rely on long-term flux measurements or satellite retrievals, which are unable to unravel impacts of changes in the associated meteorological and hydrological forcings. Modeling studies focus mainly on the aerosol-induced enhancement in diffuse radiation (e.g., Cohan et al., 2002; Gu et al., 2003; Mercado et al., 2009), but ignore other direct and indirect feedbacks such as changes in temperature and precipitation. Finally, no studies have investigated the combined effects of O_3 and aerosols or how the air pollution influences may vary in response to future emission regulations and climate change.

In this study, we assess the impacts of O_3 and aerosols on land carbon uptake in China using the global Earth system model NASA GISS ModelE2 that embeds the Yale Interactive Terrestrial Biosphere model (YIBs). This framework is known as NASA ModelE2-YIBs and fully couples the land carbon-oxidant-aerosol-climate system (Schmidt et al., 2014; Yue and Unger, 2015). The global-scale model accounts for long-range transport of pollution and large-scale feedbacks in physical climate change. The coupled Earth system simulations apply present-day and future pollution emission inventories from the Greenhouse Gas and Air Pollution Interactions and Synergies (GAINS) integrated assessment model (http://gains.iiasa.ac.at/models/). The simulations include process-based, mechanistic photosynthetic responses to physical climate change, O_3 stomatal uptake, carbon dioxide (CO_2) fertilization, and aerosol radiative perturbations, but not aerosol and acid deposition (Table 1). The O_3 and aerosol haze effects on the land carbon cycle fluxes occur predominantly through changes to gross primary productivity (GPP) and net primary productivity (NPP). Therefore, the current study focuses on GPP and NPP impacts and does not address changes in net ecosystem exchange (NEE).

2 Methods

2.1 YIBs vegetation model

The YIBs model applies the well-established Farquhar and Ball-Berry models (Farquhar et al., 1980; Ball et al., 1987) to calculate leaf photosynthesis and stomatal conductance, and adopts a canopy radiation scheme (Spitters, 1986) to separate diffuse and direct light for sunlit and shaded leaves. The assimilated carbon is dynamically allocated and stored to support leaf development (changes in leaf area index, LAI) and tree growth (changes in height). A process-based soil respiration scheme that considers carbon flows among 12 biogeochemical pools is included to simulate carbon exchange for the whole ecosystem (Yue and Unger, 2015). Similar to many terrestrial models (Schaefer et al., 2012), the current version of YIBs does not include a dynamic N cycle. Except for this deficit, the vegetation model can reasonably simulate ecosystem responses to changes in [CO_2], meteorology, phenology, and land cover (Yue et al., 2015). A semi-mechanistic O_3 vegetation damage scheme (Sitch et al., 2007) is implemented to quantify responses of photosynthesis and stomatal conductance to O_3 (Yue and Unger, 2014).

The YIBs model can be used in three different configurations: site-level, global/regional offline, and online within ModelE2-YIBs (Yue and Unger, 2015). The offline version is driven with hourly 1°×1° meteorological forcings from either the NASA Modern Era Retrospective-analysis for Research and Applications (MERRA) (Rienecker et al., 2011) or the interpolated output from ModelE2-YIBs. The online YIBs model is coupled with the climate model NASA ModelE2 (Schmidt et al., 2014), which considers the interplay among meteorology, radiation, atmospheric chemistry, and plant photosynthesis at each time step. For both global and regional simulations, 8 plant functional types (PFTs) are considered (Fig. S1). This land cover is aggregated from a dataset with 16 PFTs, which are derived using retrievals from both the Moderate Resolution Imaging Spectroradiometer (MODIS) (Hansen et al., 2003) and the Advanced Very High Resolution Radiometer (AVHRR) (Defries et al., 2000). The same vegetation cover with 16 PFTs is used by the Community Land Model (CLM) (Oleson et al., 2010).

Both the online and offline YIBs models have been extensively evaluated with site-level measurements from 145 globally-dispersed flux tower sites, long-term gridded benchmark products, and multiple satellite retrievals of LAI, tree height, phenology, and carbon fluxes (Yue and Unger, 2015; Yue et al., 2015). Driven with meteorological reanalyses, the offline YIBs vegetation model estimates a global GPP of 122.3 ± 3.1 Pg C yr^{-1}, NPP of 63.6 ± 1.9 Pg C yr^{-1}, and NEE of -2.4 ± 0.7 Pg C yr^{-1} for 1980-2011, consistent with an ensemble of land models (Yue and Unger, 2015). The online simulations with ModelE2-YIBs, including both aerosol effects and O_3 damage, yield a global GPP of 125.8 ± 3.1 Pg C yr^{-1}, NPP of 63.2 ± 0.4 Pg C yr^{-1}, and NEE of -3.0 ± 0.4 Pg C yr^{-1} under present day conditions.

2.2 NASA ModelE2-YIBs model

The NASA ModelE2-YIBs is a fully coupled chemistry-carbon-climate model with horizontal resolution of 2°×2.5° latitude by longitude and 40 vertical levels extending to 0.1 hPa. The model simulates gas-phase chemistry (NO_x, HO_x, O_x, CO, CH_4, NMVOCs), aerosols (sulfate, nitrate, elemental and organic carbon, dust, sea salt), and their interactions (Schmidt et al., 2014). Modeled oxidants influence the photochemical formation of secondary aerosol species (sulfate, nitrate, secondary organic aerosol). In turn, modeled aerosols affect photolysis rates in the online gas-phase chemistry (Schmidt et al., 2014). Heterogeneous chemistry on dust surfaces is represented (Bauer et al., 2007). The embedded radiation package includes both direct and indirect (Menon and Rotstayn, 2006) radiative effects of aerosols and considers absorption by multiple GHGs. Simulated surface solar radiation exhibits the lowest model-to-observation biases compared with the other 20 IPCC-class climate models (Wild et al., 2013). Simulated meteorological and hydrological variables have been full validated against observations and reanalysis products (Schmidt et al., 2014).

2.3 Emissions

We use global annual anthropogenic pollution inventories from the GAINS integrated assessment model (Amann et al., 2011), which compiles historic emissions of air pollutants for each country based on available international emission inventories and national information from individual countries. Inter-comparison of present-day (the year 2010) emissions (Fig. S2) shows that the GAINS V4a inventory has similar emission intensity (within ±10%) in China as IPCC RCP8.5 scenario (van Vuuren et al., 2011) for most species, except for ammonia, which is higher by 80% in GAINS. The discrepancies among different inventories emerge from varied assumptions on the stringency and effectiveness of emission control measures. While the GAINS 2010 ammonia emissions from China are larger than the RCP8.5 and HTAP emissions as shown in Fig. S2, they are close in magnitude to the year 2010 emissions of 13.84 Tg yr^{-1} estimated by the Regional Emission inventory in ASia (REAS, http://www.nies.go.jp/REAS/).

The GAINS inventory also projects medium-term variations of future emissions at five-year intervals to the year 2030. The current legislation emissions (CLE) scenario applies full implementation of national legislation affecting air pollution emissions; for China, this represents the 11^{th} five-year plan, including known failures. By 2030, in the CLE inventory, CO decreases by 18%, SO_2 by 21%, black carbon (BC) by 28%, and organic carbon (OC) by 41%, but NO_x increases by 20%, ammonia by 22%, and non-methane volatile organic compounds (NMVOC) by 6%, relative to the 2010 emission magnitude in China. To account for potential rapid changes in policy and legislation, we apply the maximum technically feasible reduction (MTFR) emission scenario as the lower limit of future air pollution. The MTFR scenario implements all currently available control technologies, disregarding implementation barriers and costs. With this scenario, the 2030 emissions of NO_x decrease by 76%, CO by 79%, SO_2 by 67%, BC by 81%, OC by 89%, ammonia by 65%, and NMVOC by 62% in China, indicating large improvement of air quality. Biomass burning emissions, adopted from the IPCC RCP8.5 scenario (van Vuuren et al., 2011), are considered as anthropogenic sources because most fire activities in China are due to human-managed prescribed burning. Compared with the GAINs inventory, present-day biomass burning is equivalent to <1% of the emissions for NO_x,

SO_2, and NH_3, 1.6% for BC, 3.0% for CO, and 9.6% for OC. By the year 2030, biomass burning emissions decrease by 1-2% for all pollution species compared with 2010.

The model represents climate-sensitive natural precursor emissions of lightning NO_x, soil NO_x and biogenic volatile organic compounds (BVOCs) (Unger and Yue, 2014). Future 2030 changes in these natural emissions are small compared to the anthropogenic emission changes. Interactive lightning NO_x emissions are calculated based on the climate model's moist convection scheme that is used to derive the total lightning and the cloud-to-ground lightning frequencies (Price et al., 1997; Pickering et al., 1998; Shindell et al., 2013). Annual average lightning NO_x emissions over China increase by 4% between 2010 and 2030. Interactive biogenic soil NO_x emission is parameterized as a function of PFT-type, soil temperature, precipitation (including pulsing events), fertilizer loss, LAI, NO_x dry deposition rate, and canopy wind speed (Yienger and Levy, 1995). Annual average biogenic soil NO_x emissions increase by only 1% over China between 2010 and 2030. Leaf isoprene emissions are simulated using a biochemical model that depends on the electron transport-limited photosynthetic rate, intercellular CO_2, canopy temperature, and atmospheric CO_2 (Unger et al., 2013). Leaf monoterpene emissions depend on canopy temperature and atmospheric CO_2 (Unger and Yue, 2014). Annual average isoprene emission in China increases by 5% (0.39 Tg C yr^{-1}) between 2010 and 2030 in response to enhanced GPP and temperature that offset the effects of CO_2-inhibition. Monoterpene emissions decrease by 5% (-0.25 Tg C) between 2010 and 2030 because CO_2-inhibition outweighs the effects of increased warming.

2.4 Simulations

2.4.1 NASA ModelE2-YIBs online

We perform 24 time-slice simulations to explore the interactive impacts of O_3 and aerosols on land carbon uptake (Table 2). All simulations are performed in atmosphere-only configuration. In these experiments, [O_3] and aerosol loading are dynamically predicted, and atmospheric chemistry processes are fully two-way coupled to the meteorology and the land biosphere. Simulations can be divided into two groups, depending on whether AIE are included. In each group, three subgroups are defined with the emission inventories of GAINS 2010, CLE 2030, and MTFR 2030 scenarios. In each subgroup, one baseline experiment is set up with only natural emissions (denoted with NAT). The other three implement all natural and anthropogenic sources of emissions (denoted with ALL), but apply different levels of O_3 damage including none (denoted with NO3), low sensitivity (LO3), and high sensitivity (HO3). To compare the differences between online and offline O_3 damage, we perform four additional simulations which do not account for the feedbacks of O_3-induced changes in biometeorology, plant growth, and ecosystem physiology. Two simulations, G10ALLHO3_OFF and G10ALLLO3_OFF, include both natural and anthropogenic emissions. The other two, G10NATHO3_OFF and G10NATLO3_OFF, include natural emissions alone.

We use prescribed sea surface temperature (SST) and sea ice distributions simulated by ModelE2 under the IPCC RCP8.5 scenario (van Vuuren et al., 2011). For these boundary conditions, we apply the monthly-varying decadal average of 2006-2015 for 2010 simulations and that of 2026-2035 for 2030 simulations. Well-mixed GHG concentrations are also adopted from the RCP8.5 scenario, with CO_2 changes from 390 ppm in 2010 to 449 ppm in 2030, and CH_4 changes from 1.779 ppm to 2.132 ppm. Land cover change projections for this scenario suggest only minor changes between the years 2010 and 2030; for example, the expansion of 3% for grassland is offset by the losses of 1% for cropland and 4% for tropical rainforest. As a result, we elect to apply the same land cover, which is derived from satellite retrievals, for both present-day and future simulations (Fig. S1). We use present-day equilibrium tree height derived from a 30-year spinup procedure (Yue and Unger, 2015) as the initial condition. All simulations are performed for 20 years, and the last 15 years are used for analyses. For simulations including effects of CO_2 fertilization, climate change, and O_3 damages, GPP and NPP reach new equilibrium within 5 years while those for NEE may require several decades due to the slow responses of the soil carbon pools (Fig. S3). The full list of simulations in Table 2 offers assessment of uncertainties due to interannual climate variability, emission inventories (CLE or MTFR), O_3 damage sensitivities (low to high), and aerosol climatic effects (direct and indirect). Uncertainties calculated based on the interannual climate variability in the model are indicated using the format 'mean ± one standard deviation'. Other sources of uncertainty are explicitly stated.

2.4.2 YIBs offline with MERRA meteorology

We perform 15 simulations to evaluate the skill of the O_3 damage scheme for vegetation in China (Table S2). Each run is driven with hourly meteorological forcings from NASA GMAO MERRA (Rienecker et al., 2011). One baseline simulation is performed without inclusion of any O_3 damage. The others, seven runs in each of two groups, are driven with fixed [O_3] at 20, 40, 60, 80, 100, 120, and 140 ppbv, respectively, using either low or high O_3 sensitivities defined by (Sitch et al., 2007). Thus, [O_3] in these offline runs is fixed without seasonal and diurnal variations to mimic field experiments that usually apply a constant level of [O_3] during the test period. We compare the O_3-affected GPP with the O_3-free GPP from the baseline simulation to derive the damaging percentages to GPP, which are compared with values for different PFTs from an ensemble of published literature results (Table S1). All simulations are performed for 1995-2011, and the last 10 years are used for analyses.

2.4.3 YIBs offline with ModelE2-YIBs meteorology

Using the offline YIBs vegetation model driven with ModelE2-YIBs meteorology, we perform 30 simulations to isolate the impacts of aerosol-induced changes in the individual meteorological drivers on carbon uptake (Table S3). Experiments are categorized into two groups, depending on whether the GCM forcings include AIE or not. In each group, three subgroups of simulations are set up with different meteorology for GAINS 2010, CLE 2030, and MTFR 2030 scenarios. Within each subgroup, five runs are designed with the different combinations of GCM forcings. One baseline run is forced with meteorology simulated without anthropogenic aerosols. The other four are additionally driven with aerosol-induced perturbations in temperature, PAR, soil moisture, or the combination of the above three variables. For these simulations, the month-to-month meteorological perturbations caused by aerosols are applied as scaling factors on the baseline forcing. The differences of NPP between sensitivity and baseline runs represent contributions of individual or total aerosol effects. Each simulation is performed for 15 years, with the last 10 years used for analyses. Uncertainties due to interannual climate variability in the model are calculated using different time periods for the online (15 years, Table 2) and offline (10 years, Table S3) runs.

3 Results

3.1 Evaluation of ModelE2-YIBs over China

3.1.1 Land carbon fluxes: GPP and NPP

To validate simulated GPP, we use a gridded benchmark product for 2009-2011 upscaled from *in situ* FLUXNET measurements (Jung et al., 2009). For NPP, we use a MODIS satellite-derived product for 2009-2011 (Zhao et al., 2005). Both datasets are interpolated to the same resolution of 2°×2.5° as ModelE2-YIBs. Simulated GPP and NPP reproduce the observed spatial patterns with high correlation coefficients (R=0.46-0.86, $p < 0.001$) and relatively low model-to-observation biases (< 20%) (Fig. 1 and Fig. S4). High values of the land carbon fluxes are predicted in the East and the Northeast, where forests and croplands dominate (Fig. S1). For GPP, prediction in the summer overestimates by 6.2% over the southern coast (< 28°N), but underestimates by 23.7% over the North China Plain (NCP, [32-40°N, 110-120°E]). Compared with the MODIS data product, predicted summer NPP is overall overestimated by 20.6% in China (Fig. 1f), with regional biases of 40.0% in the southern coast, 51.2% in the NCP, and 38.7% in the Northeast (> 124°E).

3.1.2 Surface air pollution and AOD

For surface concentrations of $PM_{2.5}$ and O_3, we use ground measurements available for 2014 from 188 sites operated by the Ministry of Environmental Protection of China (http://www.aqicn.org/). In addition, we use rural [O_3] from published literature (Table S4) to evaluate the model. For AOD, we use gridded observations of 2008-2012 from MODIS retrievals. The model simulates reasonable magnitude and spatial distribution of surface $PM_{2.5}$ concentrations (Fig. 2). Predicted AOD also reproduces the observed spatial pattern, but underestimates the high center in NCP by 24.6%. Long-term measurements of [O_3] are very limited in China. Comparisons with the 2014 one-year data from 188 urban sites show that simulated [O_3] reproduces reasonable spatial distribution but overestimates the average concentration by >40%. Such discrepancy is in part attributed to the sampling biases, because urban [O_3] is likely lower than rural [O_3] due to high NO_x emissions (NO_x titration) and aerosol loading (light extinction) in cities. Evaluations at rural sites (Table S4), which represent the major domain of China, show a mean bias of -5% (Fig. 3). The magnitude of such bias is much lower than the value of 42.5% for the comparisons at urban-dominant sites (Fig. 2f).

3.1.3 Shortwave radiation

We use ground-based observations of surface shortwave radiation and diffuse fraction from 106 pyranometer sites managed by the Climate Data Center, Chinese Meteorological Administration (Xia, 2010). Site selection is based on the availability of continuous monthly measurements during 2008-2012, resulting in 95 sites for the evaluation of total shortwave radiation. For diffuse radiation, we select the 17 sites only that provide continuous measurements during 2008-2012. Simulated surface shortwave radiation agrees well with measurements at 106 sites (Figs 4a-4c). Simulated diffuse fraction reproduces observed spatial pattern with high correlation coefficient (r = 0.74, p < 0.01), though it is on average 25.2% larger than observations (Figs 4d-4f). Such bias is mainly attributed to the overestimation in the North and Northeast. For the southeastern region, where high values of GPP dominate (Fig. 1), predicted diffuse fraction is in general within the 10% difference from the observations.

3.1.4 Ozone vegetation damage function

We adopt the same approach as Yue et al. (2016) by comparing simulated GPP-to-[O_3] responses (Table S2) with observations from multiple published literature (Table S1). We aggregate these measurements into six categories, including evergreen needleleaf forest (ENF), deciduous broadleaf forest (DBF), shrubland, C3 herbs, C4 herbs, and a mixture of all above species. We derive the sensitivity of GPP to varied [O_3] (Fig. 5) using the YIBs offline version. For most PFTs, simulated O_3 damage increases with [O_3] in broad agreement with measurements. Predicted O_3 damage reproduces observations with a correlation coefficient of 0.61 (for all samplings, n=32) and in similar magnitudes (-17.7% vs. -20.4%), suggesting that the damage scheme we adopted from Sitch et al. (2007) is ready to use in China. For the same level of [O_3], deciduous trees suffer larger damages than evergreen trees because the former species are usually more sensitive (Sitch et al., 2007) and have higher g_s (therefore higher uptake) (Wittig et al., 2007). Flux-based O_3 sensitivity for C4 herbs is only half that of C3 herbs (Sitch et al., 2007), however, concentration-based O_3 damages, both observed and simulated, are larger for C4 plants because of their higher uptake efficiency following high g_s (Yue and Unger, 2014).

3.2 O_3 effects in China

We focus our study domain in eastern China (21°-38°N, 102°-122°E, including the North China Plain, the Yangtze River Delta, and part of the Sichuan Basin), a region that suffers from high levels of O_3 and aerosols from anthropogenic pollution sources (>75% contribution; Fig. S5). We estimate that surface O_3 decreases annual GPP in China by 10.3% based on YIBs offline simulations in the absence of feedbacks from O_3 vegetation damage to meteorology and plant growth. The damage is stronger in summer, when the average GPP decreases by ~20% for both deciduous trees and C3 herbs in the East (Fig. 6). In contrast, a lower average damage to GPP of ~10% is predicted for evergreen needleleaf trees (because of low sensitivity) and C4 herbs (because of the mismatched spatial locations between C4 plants and high [O_3], Fig. S1 and Fig. 2d).

O_3 damage to photosynthesis can influence plant growth. At the same time, the O_3-induced reductions in stomatal conductance (Fig. S6a) can increase canopy temperature and inhibit plant transpiration, leading to surface warming (Fig. S6b), dry air (Fig. S6c), and rainfall deficit (Fig. S6d). These biometeorological feedbacks may in turn exacerbate the dampening of land carbon uptake. Application of ModelE2-YIBs that allows for these feedbacks gives an O_3-induced damage to annual GPP of 10.7%, a similar level to the damage computed in YIBs offline. The spatial pattern of the online O_3 inhibition also resembles that of offline damages (not shown). Sensitivity simulations with zero anthropogenic emissions show almost no O_3 damage (Fig. S7), because the [O_3] exposure from natural sources alone is usually lower than the threshold level of 40 ppbv below which the damage for most PFTs is limited (Fig. 5). Our results indicate that present-day surface O_3 causes strong inhibitions on total NPP in China, ranging from 0.43 ± 0.12 Pg C yr^{-1} with low sensitivity to 0.76 ± 0.15 Pg C yr^{-1} with high sensitivity (Table 3). The central value of NPP reduction by O_3 is 0.59 ± 0.11 Pg C yr^{-1}, assuming no direct impacts of O_3 on plant respiration. About 61% of such inhibition occurs in summer, when both photosynthesis and [O_3] reach maximum of the year.

3.3 Aerosol haze effects in China

Aerosols decrease direct solar radiation but increase diffuse radiation (Fig. S8), the latter of which is beneficial for canopy photosynthesis. The online-coupled model quantifies the concomitant meteorological and hydrological feedbacks (Fig. 7) that further influence the radiative and land carbon fluxes. Reduced insolation decreases summer surface temperature by 0.63°C in the East, inhibiting evaporation but increasing relative humidity (RH) due to the lower saturation vapor pressure (Table S5). These feedbacks combine to stimulate photosynthesis (Fig. 8a), which, in turn, strengthens plant transpiration (not shown). Atmospheric circulation and moisture convergence are also altered due to the pollution-vegetation-climate interactions, resulting in enhanced precipitation (Fig. 7b) and cloud cover (Fig. 7d). Moreover, soil moisture increases (Fig. 7f) with lower evaporation (Fig. 7e) and higher precipitation (Fig. 7b). Inclusion of AIE results in distinct climatic feedbacks (Fig. S9). Summer precipitation decreases by 0.9 mm day^{-1} (13%), leading to a 3% decline in soil moisture (Table S6). The AIE lengthens cloud lifetime and increases cloud cover, further reducing available radiation and causing a stronger surface cooling. Compared to aerosol-induced perturbations in radiation and temperature, responses in hydrological variables (e.g. precipitation and soil moisture) are usually statistically insignificant on the domain average due to the large relative interannual climate variability (Tables S5 and S6). The resulting meteorological changes over China are a combination of locally driven effects (such as changes in radiation and hence temperature) and regional-globally driven effects (such as changes in rainfall and hence soil water).

We separate the relative impacts due to aerosol-induced perturbations in temperature, radiation, and soil moisture (Fig. 8). The overall impact of the aerosol-induced biometeorological feedbacks on the carbon uptake depends on the season and vegetation type. In the summer, the aerosol-induced surface cooling brings leaf temperature closer to the photosynthetic optimum of 25°C, DRF enhances light availability of shaded leaves and LUE of sunlit leaves, and the wetter soil alleviates water stress for stoma. Consequently, aerosol-induced hydroclimatic feedbacks promote ecosystem NPP, albeit with substantial spatiotemporal variability (Fig. 8a and Table 3). Surface cooling enhances NPP in summer (Fig. 8b) but induces neutral net impacts on NPP in spring and autumn (not shown), when leaf temperature is usually below 25°C, because the cooling-driven reductions of photosynthesis are accompanied by simultaneous reductions in plant respiration. We find strong aerosol DRF in the Southeast and the Northeast, where AOD is moderate (Fig. 8c). Over the North China Plain and the Southwest, aerosol DRF is more limited. In these regions, the local background aerosol layer and/or cloud over are sufficiently optically thick that the effect of anthropogenic aerosol pollution is largely to attenuate direct sunlight and reduce NPP (Cohan et al., 2002). Aerosol-induced cooling increases soil moisture over most of the East (Fig. 7f), but the beneficial responses are confined to the Central East (Fig. 8d), where C3 crops dominate (Fig. S1). These short-root plants are more sensitive to short-term water availability than deep-root trees (Beer et al., 2010; Yue et al., 2015).

In contrast, inclusion of AIE results in detrimental impacts on NPP (Table 3). Aerosol-induced drought strongly reduces regional NPP especially over the Northeast and North China Plain (Fig. S10d), where cropland dominates (Fig. S1). Meanwhile, the increases in cloud cover reduce available radiation, leading to weakened aerosol DRF effects over the Southeast while strengthened NPP reductions in the Southwest (Fig. S10c).

3.4 Combined effects of O_3 and aerosol

Simultaneous inclusion of the aerosol effects on the land biosphere has negligible impacts on O_3 damage. The online O_3 inhibition, which is much stronger in magnitude than the aerosol effects, shows insignificant differences relative to the offline values (10.7% vs. 10.3%). As a result, we consider O_3 and aerosol effects to be linearly additive. In the year 2010, the combined effects of O_3 and aerosols (Table 3) decrease total NPP in China by 0.39 (without AIE) to 0.80 Pg C yr^{-1} (with AIE), equivalent to 9-16% of the pollution-free NPP and 16-32% of the total anthropogenic carbon emissions (Liu et al., 2015). Spatially, a dominant fraction (86% without AIE and 77% with AIE) of the reduced carbon uptake occurs in the East, where dense air pollution is co-located with high NPP (Figs 1 and 2). Temporally, a dominant fraction (60% without AIE and 52% with AIE) of the reduced carbon uptake occurs in summer, when both NPP and [O_3] reach maximum of the year. Independently, O_3 reduces NPP by 0.59 Pg C yr^{-1}, with a large range from 0.43 Pg C yr^{-1} for low damaging sensitivity to 0.76 Pg C yr^{-1} for high damaging sensitivity (Table 3). The sign of the aerosol effects is uncertain. Without AIE, aerosol is predicted to increase NPP by 0.2 Pg C yr^{-1}, because of regionally confined DRF effects and enhanced soil moisture (Fig. 8). With inclusion of AIE, aerosol decreases NPP by 0.2 Pg C yr^{-1}, mainly due to reduced soil moisture (Fig. S10). The uncertainty of individual simulations, calculated from the interannual climate variability, is usually smaller than that due to O_3 damage sensitivity and AIE (Table 3).

3.5 Future projection of pollution effects

Following the CLE scenario, by the year 2030, predicted summer [O_3] increases by 7%, while AOD decreases by 5% and surface $PM_{2.5}$ concentrations decline by 10% (Fig. 9). These changes are predominantly attributed to changes in anthropogenic emissions, as natural sources show limited changes. The reduction of AOD is related to the decreased emissions of SO_2, black carbon, and organic carbon (Fig. S2). In contrast, the enhancement of [O_3] results from the increased NO_x emissions, higher level of background CH_4 (~20%), and higher air temperature in the warmer 2030 climate. The moderate decline of aerosol loading in the 2030 CLE scenario brings benefits to land ecosystems through DRF effects (Table 3) because light scattering is often saturated in the present-day conditions due to high local AOD and regional cloud cover. Benefits from the aerosol pollution reductions are offset by worsening O_3 vegetation damage in the CLE future world (Fig. 10b). O_3-free ($[O_3]=0$) NPP increases by 14% in 2030 due to CO_2 fertilization and global climate change. Despite $[CO_2]$ increases from 390 ppm in 2010 to 449 ppm in 2030 in the RCP8.5 scenario (van Vuuren et al., 2011), which contributes to g_s inhibition of 4% on the country level, the future O_3-induced NPP damage in 2030 degrades to 14% or 0.67 Pg C yr^{-1} (Table 3), with a range from 0.43 Pg C yr^{-1} (low O_3 sensitivity) to 0.90 Pg C yr^{-1} (high O_3 sensitivity).

The MTFR scenario reflects an ambitious and optimistic future in which there is rapid global implementation of all currently available technological pollution controls. AOD decreases by 55% and $[O_3]$ decreases by 40% for this future scenario (Fig. 9). The model projects much lower damage to NPP of only 0.12 Pg C yr^{-1}, with a range from 0.06 Pg C yr^{-1} (low O_3 sensitivity) to 0.20 Pg C yr^{-1} (high O_3 sensitivity), mainly due to the 40% reduction in $[O_3]$ (Fig. 10c). Including both aerosol direct and indirect effects, O_3 and aerosols together inhibit future NPP by 0.28 Pg C yr^{-1}, ranging from 0.12 Pg C yr^{-1} with low O_3 sensitivity to 0.43 Pg C yr^{-1} with high O_3 sensitivity. As a result, The MTFR scenario offers strong recovery of the land carbon uptake in China by 2030.

4. Discussion

4.1 Comparison with previous estimates

Previous estimates of O_3 damages over the whole China region are very limited. Two important studies, Tian et al. (2011) and Ren et al. (2011), have quantified the impacts of surface O_3 on carbon assimilation in China. Both studies applied the dynamic land ecosystem model (DLEM) with O_3 damage scheme proposed by Felzer et al. (2004), except that Tian et al. (2011) focused on NEE while Ren et al. (2011) also investigated NPP. The Felzer et al. (2004) scheme calculates O_3 uptake based on stomatal conductance and the AOT40 (accumulated hourly O_3 dose over a threshold of 40 ppb).

Yue and Unger (2014) estimated O_3-induced reductions in GPP over U.S. using Sitch et al. (2007) scheme and found an average value of 4-8% (low to high sensitivity), consistent with the reduction of 3-7% in Felzer et al. (2004). For this study, we estimate that present-day O_3 decreases NPP by 0.43-0.76 Pg C yr^{-1}, higher than the 0.42 Pg C yr^{-1} calculated by Ren et al. (2011). However, the percentage reduction of 10.1-17.8% in our estimate is weaker than the value of 24.7% in Ren et al. (2011). The main reason for such discrepancy lies in the differences in the climatological NPP. Combining all environmental drivers (e.g. [CO_2], meteorology, [O_3], and aerosols), we predict an average NPP of 3.98 ± 0.1 Pg C yr^{-1} for the year 2010 (uncertainties from AIE) with the ModelE2-YIBs model. This value is close to the average of 3.35 ± 1.25 Pg C yr^{-1} for 1981-2000 calculated based on 54 estimates from 33 studies (Shao et al., 2016). Using DLEM, Ren et al. (2011) estimated an optimal NPP of 1.67 Pg C yr^{-1} for 2000-2005 over China, which is only half of the literature-based estimate.

In the absence of any previous studies of aerosol pollution effects on land carbon uptake in China, our strategy is to compare separately the simulated aerosol climatic feedback (climate sensitivity) and simulated NPP response to climate variability (NPP sensitivity) with existing published results. ModelE2-YIBs simulates an annual reduction of 26.2 W m^{-2} in all-sky surface solar radiation over the East due to aerosols pollution (Table S5), similar to the estimate of 28 W m^{-2} by Folini and Wild (2015). In response to this radiative perturbation, aerosol pollution causes a widespread cooling of 0.3-0.9 °C in summer over the East (Fig. 7a), consistent with estimates of 0-0.9 °C by Qian et al. (2003), 0-0.7 °C by Liu et al. (2009), and average of 0.5 °C by Folini and Wild (2015). Aerosol pollution effects on regional precipitation patterns in China are not well understood due to different climate model treatments of land-atmosphere interactions and the interplay between regional and large-scale circulation. In ModelE2-YIBs, without AIE, aerosol induces a "northern drought and southern flood" pattern in agreement with Gu et al. (2006), but different to Liu et al. (2009) who predicted widespread drought instead. Including both aerosol direct and indirect effects, ModelE2-YIBs simulates an average reduction of 0.48 mm day^{-1} in summer rainfall widespread over China (Fig. S9b), similar to the magnitude of 0.4 mm day^{-1} estimated with the ECHAM5-HAM model

(Folini and Wild, 2015), but higher than the 0.21 mm day^{-1} predicted by the RegCM2 model (Huang et al., 2007).

Sensitivity experiments with YIBs show that summer NPP increases following aerosol-induced changes in temperature, radiation, and precipitation (Fig. 8). The cooling-related NPP enhancement (Fig. 8b) collocates with changes in temperature (Fig. 7a), indicating that sensitivity of NPP to temperature is negative over eastern China. Such temperature sensitivity is consistent with the ensemble estimate based on 10 terrestrial models (Piao et al., 2013). For the aerosol-induced radiative perturbation, many studies have shown that moderate aerosol/cloud amount promotes plant photosynthesis through enhanced DRF, while dense aerosol/cloud decreases carbon uptake due to light extinction (Cohan et al., 2002; Gu et al., 2003; Rocha et al., 2004; Alton, 2008; Knohl and Baldocchi, 2008; Mercado et al., 2009; Jing et al., 2010; Bai et al., 2012; Cirino et al., 2014; Strada et al., 2015). Theoretically, at each specific land location on the Earth, there is an AOD threshold below which aerosol promotes local NPP. The threshold is dependent on latitude, cloud/aerosol amount, and plant types. In a related study by Yue and Unger (2017), we applied a well-validated offline radiation model to calculate these AOD thresholds over China. We conclude that present-day AOD is lower than the local thresholds in the Northeast and Southeast but exceeds the thresholds in the North China Plain, explaining why aerosol-induced diming enhances NPP in the former regions but reduces NPP in the latter (Fig. 8c). On the country level, the NPP enhancement due to aerosol DRF is 0.07 Pg C yr^{-1} in Yue and Unger (2017), very close to the 0.09 Pg C yr^{-1} estimated with ModelE2-YIBs model (Table 2).

4.2 Uncertainties

A major source of uncertainty originates from the paucity of observations. For instance, direct measurements of aerosol pollution effects on NPP are non-existent for China. The aerosol effects involve complex interactions that challenge the field-based validation of the underlying independent processes. Field experiments of O_3 vegetation damage are becoming more available, but their applications are limited by the large variations in the species-specific responses (Lombardozzi et al., 2013), as well as the discrepancies in the treatments of [O_3] enhancement (Wittig et al., 2007). Instead of equally using all individual records from multiple literatures (Lombardozzi et al., 2013), we aggregate O_3 damage for each literature based on the seasonal (or growth-season) average. In this way, the derived PFT-level GPP-[O_3] relationships are not biased towards the experiments with a large number of samplings. Such aggregation also reduces sampling noise and allows construction of the quantified GPP-[O_3] relationships used for model assessment. Predicted [O_3] is largely overestimated at urban sites but exhibits reasonable magnitude at rural sites (Figs 2 and 3). Measurements of background [O_3] in China are limited both in space and time, restricting comprehensive validation of [O_3] and the consequent estimate of O_3 damages on the country level.

We have estimated O_3 damages to NPP (instead of GPP), an optimal indicator for net carbon uptake by plants. Our calculations assume no impacts of O_3 on autotrophic respiration. Yet, limited observations have found increased plant respiration in response to O_3 injury (Felzer et al., 2007), suggesting that our calculation of O_3-induced NPP reductions might be underestimated. Current large mechanistic uncertainties in the role of anthropogenic nitrogen (N) deposition to China's land carbon uptake (Tian et al., 2011; Xiao et al., 2015) have prohibited the inclusion of dynamic carbon-nitrogen coupling in the Earth system model used here. Previous studies have suggested that inclusion of N fertilization can relieve or offset damages by O_3, especially for N-limited forests (Ollinger et al., 2002). Relative to the present day, atmospheric reactive N deposition increases by 20% in the CLE scenario but decreases by 60% in the MTFR scenario, suggesting that the stronger O_3 damage in CLE might be overestimated while the reduced damage in MTFR might be too optimistic.

Our estimate of NPP responses to aerosol pollution is sensitive to modeling uncertainties in concentration, radiation, and climatic effects. Simulated surface $PM_{2.5}$ is reasonable but AOD is underestimated in the North China Plain (Fig. 2), likely because of the biases in aerosol optical parameters. Using a different set of optical parameters, we predicted much higher AOD that is closer to observations with the same aerosol vertical profile and particle compositions (Yue and Unger, 2017). The model overestimates diffuse fraction in China (Fig. 4), likely because of simulated biases in clouds. Previously, we improved the prediction of diffuse fraction in China using observed cloud profiles for the region (Yue and Unger, 2017). Biases in simulated AOD and diffuse fraction introduce uncertainties in the aerosol DRF especially in the affected localized model grid cells. Yet, averaged over the China domain, our estimate of NPP change by aerosol DRF (0.09 Pg C yr^{-1}) is consistent with the previous assessment in Yue and Unger (2017) (0.07 Pg C yr^{-1}). Aerosol-induced impacts on precipitation and soil moisture are not statistically significant over the regionally averaged domain (Tables S5 and S6). However, for the 2010 and 2030 CLE cases with AIE, 2 out of 6 scenarios, the aerosol-induced impact on soil moisture dominates the total NPP response (Table 3). Furthermore, the relatively coarse resolution of the global model and usage of emission inventories may introduce additional biases and exacerbate the total uncertainties.

Importantly, our estimate of NPP response to aerosol effects, with or without AIE, is secondary in magnitude compared to the O_3 vegetation damage, suggesting that the net impact of current air pollution levels in China is detrimental to the land carbon uptake there. Locally, this pollution damage exerts a threat to plant health, terrestrial ecosystem services, and food production. Globally, air pollution effects may enhance planetary warming by decreasing the land removal rate of atmospheric CO_2. Our results show substantial benefits to the protection of plant health and the regional land carbon sink in China from stringent air pollution controls, especially for O_3 precursors. Our analysis highlights the complex interplay between immediate and more local pollution issues, and longer-term global warming. Future air pollution controls provide an additional co-benefit to human society: the offsetting of fossil fuel CO_2 emissions through enhanced land sequestration of atmospheric CO_2.

Acknowledgements. The authors are grateful to Prof. William Collins and an anonymous reviewer for constructive comments improving this paper. X. Yue acknowledges funding support from the National Basic Research Program of China (973 program, Grant No. 2014CB441202) and the “Thousand Youth Talents Plan”. This research was supported in part by the facilities and staff of the Yale University Faculty of Arts and Sciences High Performance Computing Center.

References

Ainsworth, E. A., Yendrek, C. R., Sitch, S., Collins, W. J., and Emberson, L. D.: The Effects of Tropospheric Ozone on Net Primary Productivity and Implications for Climate Change, Annual Review of Plant Biology, Vol 63, 63, 637-661, doi:10.1146/Annurev-Arplant-042110-103829, 2012.

Alton, P. B.: Reduced carbon sequestration in terrestrial ecosystems under overcast skies compared to clear skies, Agricultural and Forest Meteorology, 148, 1641–1653, doi:10.1016/j.agrformet.2008.05.014, 2008.

Amann, M., Bertok, I., Borken-Kleefeld, J., Cofala, J., Heyes, C., Hoglund-Isaksson, L., Klimont, Z., Nguyen, B., Posch, M., Rafaj, P., Sandler, R., Schopp, W., Wagner, F., and Winiwarter, W.: Cost-effective control of air quality and greenhouse gases in Europe: Modeling and policy applications, Environmental Modelling & Software, 26, 1489-1501, doi:10.1016/j.envsoft.2011.07.012, 2011.

Bai, Y., Wang, J., Zhang, B., Zhang, Z., and Liang, J.: Comparing the impact of cloudiness on carbon dioxide exchange in a grassland and a maize cropland in northwestern China, Ecological Research, 27, 615-623, doi:10.1007/s11284-012-0930-z, 2012.

Ball, J. T., Woodrow, I. E., and Berry, J. A.: A model predicting stomatal conductance and its contribution to the control of photosyn- thesis under different environmental conditions, in: Progress in Photosynthesis Research, edited by: Biggins, J., Nijhoff, Dordrecht, Netherlands, 110–112, 1987.

Bauer, S. E., Mishchenko, M. I., Lacis, A. A., Zhang, S., Perlwitz, J., and Metzger, S. M.: Do sulfate and nitrate coatings on mineral dust have important effects on radiative properties and climate modeling?, Journal of Geophysical Research, 112, D06307 doi:10.1029/2005JD006977, 2007.

Beer, C., Reichstein, M., Tomelleri, E., Ciais, P., Jung, M., Carvalhais, N., Rodenbeck, C., Arain, M. A., Baldocchi, D., Bonan, G. B., Bondeau, A., Cescatti, A., Lasslop, G., Lindroth, A., Lomas, M., Luyssaert, S., Margolis, H., Oleson, K. W., Roupsard, O., Veenendaal, E., Viovy, N., Williams, C., Woodward, F. I., and Papale, D.: Terrestrial Gross Carbon Dioxide Uptake: Global Distribution and Covariation with Climate, Science, 329, 834-838, doi:10.1126/Science.1184984, 2010.

Cirino, G. G., Souza, R. A. F., Adams, D. K., and Artaxo, P.: The effect of atmospheric aerosol particles and clouds on net ecosystem exchange in the Amazon, Atmospheric Chemistry and Physics, 14, 6523-6543, doi:10.5194/acp-14-6523-2014, 2014.

Cohan, D. S., Xu, J., Greenwald, R., Bergin, M. H., and Chameides, W. L.: Impact of atmospheric aerosol light scattering and absorption on terrestrial net primary productivity, Global Biogeochemical Cycles, 16, 1090, doi:10.1029/2001gb001441, 2002.

Defries, R. S., Hansen, M. C., Townshend, J. R. G., Janetos, A. C., and Loveland, T. R.: A new global 1-km dataset of percentage tree cover derived from remote sensing, Global Change Biology, 6, 247-254, doi:10.1046/J.1365-2486.2000.00296.X, 2000.

Farquhar, G. D., Caemmerer, S. V., and Berry, J. A.: A Biochemical-Model of Photosynthetic Co2 Assimilation in Leaves of C-3 Species, Planta, 149, 78-90, doi:10.1007/Bf00386231, 1980.

Felzer, B., Kicklighter, D., Melillo, J., Wang, C., Zhuang, Q., and Prinn, R.: Effects of ozone on net primary production and carbon sequestration in the conterminous

United States using a biogeochemistry model, Tellus Series B-Chemical and Physical Meteorology, 56, 230-248, doi:Doi 10.1111/J.1600-0889.2004.00097.X, 2004.

Felzer, B. S., Cronin, T., Reilly, J. M., Melillo, J. M., and Wang, X.: Impacts of ozone on trees and crops, C. R. Geoscience, 229, doi:10.1016/j.crte.2007.08.008, 2007.

Folini, D., and Wild, M.: The effect of aerosols and sea surface temperature on China's climate in the late twentieth century from ensembles of global climate simulations, J. Geophys. Res., 12, 2261-2279, doi:10.1002/2014JD022851, 2015.

Gu, L. H., Baldocchi, D. D., Wofsy, S. C., Munger, J. W., Michalsky, J. J., Urbanski, S. P., and Boden, T. A.: Response of a deciduous forest to the Mount Pinatubo eruption: Enhanced photosynthesis, Science, 299, 2035-2038, doi:10.1126/science.1078366, 2003.

Gu, Y., Liou, K. N., Xue, Y., Mechoso, C. R., Li, W., and Luo, Y.: Climatic effects of different aerosol types in China simulated by the UCLA general circulation model, Journal of Geophysical Research, 111, D15201, doi:10.1029/2005JD006312, 2006.

Hansen, M. C., DeFries, R. S., Townshend, J. R. G., Carroll, M., Dimiceli, C., and Sohlberg, R. A.: Global Percent Tree Cover at a Spatial Resolution of 500 Meters: First Results of the MODIS Vegetation Continuous Fields Algorithm, Earth Interactions, 7, 1-15, doi:10.1175/1087-3562(2003)007<0001:GPTCAA>2.0.CO;2, 2003.

Huang, Y., Chameides, W. L., and Dickinson, R. E.: Direct and indirect effects of anthropogenic aerosols on regional precipitation over east Asia, Journal of Geophysical Research, 112, D03212, doi:10.1029/2006JD007114, 2007.

Jing, X., Huang, J., Wang, G., Higuchi, K., Bi, J., Sun, Y., Yu, H., and Wang, T.: The effects of clouds and aerosols on net ecosystem CO2 exchange over semi-arid Loess Plateau of Northwest China, Atmospheric Chemistry and Physics, 10, 8205-8218, doi:10.5194/acp-10-8205-2010, 2010.

Jung, M., Reichstein, M., and Bondeau, A.: Towards global empirical upscaling of FLUXNET eddy covariance observations: validation of a model tree ensemble approach using a biosphere model, Biogeosciences, 6, 2001-2013, doi:10.5194/bg-6-2001-2009, 2009.

Kanniah, K. D., Beringer, J., North, P., and Hutley, L.: Control of atmospheric particles on diffuse radiation and terrestrial plant productivity: A review, Progress in Physical Geography, 36, 209-237, doi:10.1177/0309133311434244, 2012.

Knohl, A., and Baldocchi, D. D.: Effects of diffuse radiation on canopy gas exchange processes in a forest ecosystem, Journal of Geophysical Research, 113, G02023, doi:10.1029/2007JG000663, 2008.

Liu, Y., Sun, J., and Yang, B.: The effects of black carbon and sulphate aerosols in China regions on East Asia monsoons, Tellus Series B-Chemical and Physical Meteorology, 61B, 642-656, doi:10.1111/j.1600-0889.2009.00427.x, 2009.

Liu, Z., Guan, D. B., Wei, W., Davis, S. J., Ciais, P., Bai, J., Peng, S. S., Zhang, Q., Hubacek, K., Marland, G., Andres, R. J., Crawford-Brown, D., Lin, J. T., Zhao, H. Y., Hong, C. P., Boden, T. A., Feng, K. S., Peters, G. P., Xi, F. M., Liu, J. G., Li, Y., Zhao, Y., Zeng, N., and He, K. B.: Reduced carbon emission estimates from fossil fuel combustion and cement production in China, Nature, 524, 335-338, doi:10.1038/nature14677, 2015.

Lombardozzi, D., Sparks, J. P., and Bonan, G.: Integrating O3 influences on terrestrial processes: photosynthetic and stomatal response data available for regional and global modeling, Biogeosciences, 10, 6815-6831, doi:10.5194/bg-10-6815-2013, 2013.

Menon, S., and Rotstayn, L.: The radiative influence of aerosol effects on liquid-phase cumulus and stratiform clouds based on sensitivity studies with two climate models, Climate Dynamics, 27, 345-356, doi:10.1007/s00382-006-0139-3, 2006.

Mercado, L. M., Bellouin, N., Sitch, S., Boucher, O., Huntingford, C., Wild, M., and Cox, P. M.: Impact of changes in diffuse radiation on the global land carbon sink, Nature, 458, 1014-1017, doi:Doi 10.1038/Nature07949, 2009.

Oleson, K. W., Lawrence, D. M., Bonan, G. B., Flanne, M. G., Kluzek, E., Lawrence, P. J., Levis, S., Swenson, S. C., and Thornton, P. E.: Technical Description of version 4.0 of the Community Land Model (CLM), National Center for Atmospheric Research, Boulder, CONCAR/TN-478+STR, 2010.

Ollinger, S. V., Aber, J. D., Reich, P. B., and Freuder, R. J.: Interactive effects of nitrogen deposition, tropospheric ozone, elevated CO2 and land use history on the carbon dynamics of northern hardwood forests, Global Change Biology, 8, 545-562, doi:10.1046/J.1365-2486.2002.00482.X, 2002.

Piao, S. L., Fang, J. Y., Ciais, P., Peylin, P., Huang, Y., Sitch, S., and Wang, T.: The carbon balance of terrestrial ecosystems in China, Nature, 458, 1009-1013, doi:10.1038/nature07944, 2009.

Piao, S. L., Sitch, S., Ciais, P., Friedlingstein, P., Peylin, P., Wang, X. H., Ahlstrom, A., Anav, A., Canadell, J. G., Cong, N., Huntingford, C., Jung, M., Levis, S., Levy, P. E., Li, J. S., Lin, X., Lomas, M. R., Lu, M., Luo, Y. Q., Ma, Y. C., Myneni, R. B., Poulter, B., Sun, Z. Z., Wang, T., Viovy, N., Zaehle, S., and Zeng, N.: Evaluation of terrestrial carbon cycle models for their response to climate variability and to CO2 trends, Global Change Biology, 19, 2117-2132, doi:10.1111/Gcb.12187, 2013.

Pickering, K. E., Wang, Y., Tao, W.-K., Price, C., and Müller, J.-F.: Vertical distributions of lightning NOx for use in regional and global chemical transport models, Journal of Geophysical Research, 103, 31203–31216, doi:10.1029/98JD02651, 1998.

Price, C., Penner, J., and Prather, M.: NOx from lightning: 1. Global distribution based on lightning physics, Journal of Geophysical Research, 102, 5929–5941, doi:10.1029/96JD03504, 1997.

Qian, Y., Leung, L. R., Ghan, S. J., and Giorgi, F.: Regional climate effects of aerosols over China: modeling and observation, Tellus Series B-Chemical and Physical Meteorology, 55, 914-934, doi:10.1046/j.1435-6935.2003.00070.x, 2003.

Reich, P. B., and Amundson, R. G.: Ambient Levels of Ozone Reduce Net Photosynthesis in Tree and Crop Species, Science, 230, 566-570, doi:10.1126/science.230.4725.566, 1985.

Ren, W., Tian, H., Tao, B., Chappelka, A., Sun, G., Lu, C., Liu, M., Chen, G., and Xu, X.: Impacts of tropospheric ozone and climate change on net primary productivity and net carbon exchange of China's forest ecosystems, Global Ecology & Biogeography, 20, 391-406, doi:10.1111/j.1466-8238.2010.00606.x, 2011.

Rienecker, M. M., Suarez, M. J., Gelaro, R., Todling, R., Bacmeister, J., Liu, E., Bosilovich, M. G., Schubert, S. D., Takacs, L., Kim, G. K., Bloom, S., Chen, J. Y., Collins, D., Conaty, A., Da Silva, A., Gu, W., Joiner, J., Koster, R. D., Lucchesi, R.,

Molod, A., Owens, T., Pawson, S., Pegion, P., Redder, C. R., Reichle, R., Robertson, F. R., Ruddick, A. G., Sienkiewicz, M., and Woollen, J.: MERRA: NASA's Modern-Era Retrospective Analysis for Research and Applications, Journal of Climate, 24, 3624-3648, doi:10.1175/Jcli-D-11-00015.1, 2011.
Rocha, A. V., Su, H. B., Vogel, C. S., Schmid, H. P., and Curtis, P. S.: Photosynthetic and water use efficiency responses to diffuse radiation by an aspen-dominated northern hardwood forest, Forest Science, 50, 793-801, 2004.
Schaefer, K., Schwalm, C. R., Williams, C., Arain, M. A., Barr, A., Chen, J. M., Davis, K. J., Dimitrov, D., Hilton, T. W., Hollinger, D. Y., Humphreys, E., Poulter, B., Raczka, B. M., Richardson, A. D., Sahoo, A., Thornton, P., Vargas, R., Verbeeck, H., Anderson, R., Baker, I., Black, T. A., Bolstad, P., Chen, J. Q., Curtis, P. S., Desai, A. R., Dietze, M., Dragoni, D., Gough, C., Grant, R. F., Gu, L. H., Jain, A., Kucharik, C., Law, B., Liu, S. G., Lokipitiya, E., Margolis, H. A., Matamala, R., McCaughey, J. H., Monson, R., Munger, J. W., Oechel, W., Peng, C. H., Price, D. T., Ricciuto, D., Riley, W. J., Roulet, N., Tian, H. Q., Tonitto, C., Torn, M., Weng, E. S., and Zhou, X. L.: A model-data comparison of gross primary productivity: Results from the North American Carbon Program site synthesis, J. Geophys. Res., 117, G03010, doi:10.1029/2012jg001960, 2012.
Schmidt, G. A., Kelley, M., Nazarenko, L., Ruedy, R., Russell, G. L., Aleinov, I., Bauer, M., Bauer, S. E., Bhat, M. K., Bleck, R., Canuto, V., Chen, Y. H., Cheng, Y., Clune, T. L., Del Genio, A., de Fainchtein, R., Faluvegi, G., Hansen, J. E., Healy, R. J., Kiang, N. Y., Koch, D., Lacis, A. A., LeGrande, A. N., Lerner, J., Lo, K. K., Matthews, E. E., Menon, S., Miller, R. L., Oinas, V., Oloso, A. O., Perlwitz, J. P., Puma, M. J., Putman, W. M., Rind, D., Romanou, A., Sato, M., Shindell, D. T., Sun, S., Syed, R. A., Tausnev, N., Tsigaridis, K., Unger, N., Voulgarakis, A., Yao, M. S., and Zhang, J. L.: Configuration and assessment of the GISS ModelE2 contributions to the CMIP5 archive, Journal of Advances in Modeling Earth Systems, 6, 141-184, doi:10.1002/2013ms000265, 2014.
Shao, J., Zhou, X. H., Luo, Y. Q., Zhang, G. D., Yan, W., Li, J. X., Li, B., Dan, L., Fisher, J. B., Gao, Z. Q., He, Y., Huntzinger, D., Jain, A. K., Mao, J. F., Meng, J. H., Michalak, A. M., Parazoo, N. C., Peng, C. H., Poulter, B., Schwalm, C. R., Shi, X. Y., Sun, R., Tao, F. L., Tian, H. Q., Wei, Y. X., Zeng, N., Zhu, Q., and Zhu, W. Q.: Uncertainty analysis of terrestrial net primary productivity and net biome productivity in China during 1901-2005, Journal of Geophysical Research, 121, 1372-1393, doi:10.1002/2015jg003062, 2016.
Shindell, D. T., Pechony, O., Voulgarakis, A., Faluvegi, G., Nazarenko, L., Lamarque, J. F., Bowman, K., Milly, G., Kovari, B., Ruedy, R., and Schmidt, G. A.: Interactive ozone and methane chemistry in GISS-E2 historical and future climate simulations, Atmospheric Chemistry and Physics, 13, 2653-2689, doi:10.5194/Acp-13-2653-2013, 2013.
Sitch, S., Cox, P. M., Collins, W. J., and Huntingford, C.: Indirect radiative forcing of climate change through ozone effects on the land-carbon sink, Nature, 448, 791-794, doi:10.1038/Nature06059, 2007.
Spitters, C. J. T.: Separating the Diffuse and Direct Component of Global Radiation and Its Implications for Modeling Canopy Photosynthesis .2. Calculation of Canopy

Photosynthesis, Agricultural and Forest Meteorology, 38, 231-242, doi:10.1016/0168-1923(86)90061-4, 1986.

Spracklen, D. V., Arnold, S. R., and Taylor, C. M.: Observations of increased tropical rainfall preceded by air passage over forests, Nature, 489, 282-285, doi:10.1038/nature11390, 2012.

Steiner, A. L., and Chameides, W. L.: Aerosol-induced thermal effects increase modelled terrestrial photosynthesis and transpiration, Tellus Series B-Chemical and Physical Meteorology, 57, 404-411, doi:DOI 10.1111/j.1600-0889.2005.00158.x, 2005.

Strada, S., Unger, N., and Yue, X.: Observed aerosol-induced radiative effect on plant productivity in the eastern United States, Atmospheric Environment, 122, 463–476, doi:10.1016/j.atmosenv.2015.09.051, 2015.

Tian, H. Q., Melillo, J., Lu, C. Q., Kicklighter, D., Liu, M. L., Ren, W., Xu, X. F., Chen, G. S., Zhang, C., Pan, S. F., Liu, J. Y., and Running, S.: China's terrestrial carbon balance: Contributions from multiple global change factors, Global Biogeochemical Cycles, 25, Gb1007, doi:10.1029/2010gb003838, 2011.

Unger, N., Harper, K., Zheng, Y., Kiang, N. Y., Aleinov, I., Arneth, A., Schurgers, G., Amelynck, C., Goldstein, A., Guenther, A., Heinesch, B., Hewitt, C. N., Karl, T., Laffineur, Q., Langford, B., McKinney, K. A., Misztal, P., Potosnak, M., Rinne, J., Pressley, S., Schoon, N., and Serça, D.: Photosynthesis-dependent isoprene emission from leaf to planet in a global carbon–chemistry–climate model, Atmos. Chem. Phys., 13, 17717-17791, doi:10.5194/acp-13-10243-2013, 2013.

Unger, N., and Yue, X.: Strong chemistry-climate feedbacks in the Pliocene, Geophysical Research Letters, 41, 527-533, doi:10.1002/2013gl058773, 2014.

van Vuuren, D. P., Edmonds, J., Kainuma, M., Riahi, K., Thomson, A., Hibbard, K., Hurtt, G. C., Kram, T., Krey, V., Lamarque, J. F., Masui, T., Meinshausen, M., Nakicenovic, N., Smith, S. J., and Rose, S. K.: The representative concentration pathways: an overview, Climatic Change, 109, 5-31, doi:10.1007/s10584-011-0148-z, 2011.

Wild, M., Folini, D., Schar, C., Loeb, N., Dutton, E. G., and Konig-Langlo, G.: The global energy balance from a surface perspective, Climate Dynamics, 40, 3107-3134, doi:10.1007/s00382-012-1569-8, 2013.

Wittig, V. E., Ainsworth, E. A., and Long, S. P.: To what extent do current and projected increases in surface ozone affect photosynthesis and stomatal conductance of trees? A meta-analytic review of the last 3 decades of experiments, Plant Cell and Environment, 30, 1150-1162, doi:10.1111/J.1365-3040.2007.01717.X, 2007.

Xia, X.: A closer looking at dimming and brightening in China during 1961-2005, Annales Geophysicae, 28, 1121-1132, doi:10.5194/angeo-28-1121-2010, 2010.

Xiao, J. F., Zhou, Y., and Zhang, L.: Contributions of natural and human factors to increases in vegetation productivity in China, Ecosphere, 6, 233, doi:10.1890/Es14-00394.1, 2015.

Yienger, J. J., and Levy, H.: Empirical-Model of Global Soil-Biogenic Nox Emissions, J. Geophys. Res., 100, 11447-11464, doi:10.1029/95jd00370, 1995.

Yue, X., and Unger, N.: Ozone vegetation damage effects on gross primary productivity in the United States, Atmospheric Chemistry and Physics, 14, 9137-9153, doi:10.5194/acp-14-9137-2014, 2014.

Yue, X., and Unger, N.: The Yale Interactive terrestrial Biosphere model version 1.0: description, evaluation and implementation into NASA GISS ModelE2, Geoscientific Model Development, 8, 2399-2417, doi:10.5194/gmd-8-2399-2015, 2015.
Yue, X., Unger, N., and Zheng, Y.: Distinguishing the drivers of trends in land carbon fluxes and biogenic emissions over the past three decades, Atmospheric Chemistry and Physics, 15, 11931-11948, doi:10.5194/acp-15-11931-2015, 2015.
Yue, X., Keenan, T. F., Munger, W., and Unger, N.: Limited effect of ozone reductions on the 20-year photosynthesis trend at Harvard forest, Global Change Biology, 22, 3750-3759, doi:10.1111/gcb.13300, 2016.
Yue, X., and Unger, N.: Aerosol optical depth thresholds as a tool to assess diffuse radiation fertilization of the land carbon uptake in China, Atmospheric Chemistry and Physics, 17, 1329-1342, doi:10.5194/acp-17-1329-2017, 2017.
Zhao, M. S., Heinsch, F. A., Nemani, R. R., and Running, S. W.: Improvements of the MODIS terrestrial gross and net primary production global data set, Remote Sensing of Environment, 95, 164-176, doi:10.1016/J.Rse.2004.12.011, 2005.

Table 1. Summary of models and simulations

Model Name	Model class	Climate drivers	Number of runs	Table index [a]	Purpose
ModelE2-YIBs	Coupled climate model	Online	24	2	Calculate ΔNPP by O_3 and aerosols at 2010 and 2030
YIBs	Vegetation model	MERRA	15	S2	Evaluate O_3 damage scheme for China PFTs
YIBs	Vegetation model	ModelE2 -YIBs	30	S3	Isolate aerosol individual climatic impacts on NPP

[a] Table index refers to the tables in the main text and supporting information.

Table 2. Summary of 24 online simulations with the ModelE2-YIBs model

Simulations	Period	Emission Inventories	Emission sources	Ozone damage	Aerosol indirect effect
G10NATNO3	2010	GAINS [a]	Natural	Null	No
G10ALLNO3	2010	GAINS	All [d]	Null	No
G10ALLLO3	2010	GAINS	All	Low	No
G10ALLHO3	2010	GAINS	All	High	No
G30NATNO3	2030	GAINS CLE [b]	Natural	Null	No
G30ALLNO3	2030	GAINS CLE	All	Null	No
G30ALLLO3	2030	GAINS CLE	All	Low	No
G30ALLHO3	2030	GAINS CLE	All	High	No
M30NATNO3	2030	GAINS MTFR [c]	Natural	Null	No
M30ALLNO3	2030	GAINS MTFR	All	Null	No
M30ALLLO3	2030	GAINS MTFR	All	Low	No
M30ALLHO3	2030	GAINS MTFR	All	High	No
G10NATNO3_AIE	2010	GAINS	Natural	Null	Yes
G10ALLNO3_AIE	2010	GAINS	All	Null	Yes
G10ALLLO3_AIE	2010	GAINS	All	Low	Yes
G10ALLHO3_AIE	2010	GAINS	All	High	Yes
G30NATNO3_AIE	2030	GAINS CLE	Natural	Null	Yes
G30ALLNO3_AIE	2030	GAINS CLE	All	Null	Yes
G30ALLLO3_AIE	2030	GAINS CLE	All	Low	Yes
G30ALLHO3_AIE	2030	GAINS CLE	All	High	Yes
M30NATNO3_AIE	2030	GAINS MTFR	Natural	Null	Yes
M30ALLNO3_AIE	2030	GAINS MTFR	All	Null	Yes
M30ALLLO3_AIE	2030	GAINS MTFR	All	Low	Yes
M30ALLHO3_AIE	2030	GAINS MTFR	All	High	Yes

[a] GAINS is short for the v4a emission inventory of Greenhouse Gas and Air Pollution Interactions and Synergies (http://gains.iiasa.ac.at/models/index.html).

[b] CLE is the emission scenario predicted based on current legislation emissions.

[c] MTFR is the emission scenario predicted with maximum technically feasible reductions.

[d] All emissions including both natural and anthropogenic sources. For the detailed anthropogenic emissions, refer to Fig. S2.

Table 3. Changes in NPP over China due to combined and separate effects [a] of air pollution (units: Pg C yr^{-1})

	2010	2030 CLE	2030 MTFR
O_3 (mean) [b]	**-0.59 ± 0.11 (-0.60 ± 0.13)**	**-0.67 ± 0.11 (-0.71 ± 0.16)**	**-0.29 ± 0.14 (-0.31 ± 0.10)**
Low sensitivity	-0.43 ± 0.12 (-0.40 ± 0.13)	-0.43 ± 0.14 (-0.51 ± 0.16)	-0.22 ± 0.17 (-0.15 ± 0.10)
High sensitivity	-0.76 ± 0.15 (-0.80 ± 0.16)	-0.90 ± 0.13 (-0.92 ± 0.18)	-0.36 ± 0.16 (-0.46 ± 0.12)
Aerosol (total) [c]	**0.20 ± 0.08 (-0.20 ± 0.09)**	**0.23 ± 0.14 (-0.09 ± 0.19)**	**0.16 ± 0.14 (0.04 ± 0.17)**
Temperature [d]	0.03 ± 0.04 (0.01 ± 0.04)	0.04 ± 0.02 (0.02 ± 0.05)	0.03 ± 0.04 (0.00 ± 0.04)
Radiation [d]	0.09 ± 0.04 (-0.03 ± 0.04)	0.16 ± 0.06 (-0.01 ± 0.06)	0.11 ± 0.04 (-0.03 ± 0.03)
Soil moisture [d]	0.07 ± 0.07 (-0.19 ± 0.10)	0.01 ± 0.09 (-0.09 ± 0.15)	0.03 ± 0.12 (0.00 ± 0.09)
O_3 + aerosol (net) [e]	**-0.39 ± 0.12 (-0.80 ± 0.11)**	**-0.43 ± 0.12 (-0.80 ± 0.10)**	**-0.12 ± 0.13 (-0.28 ± 0.14)**

[a] Results shown are the averages ± one standard deviation. Simulations with both aerosol direct and indirect radiative effects (AIE) are shown in the brackets.

[b] Mean O_3 damages are calculated as half of differences in ΔNPP between low and high sensitivities, e.g., present-day mean O_3 damage is $\frac{1}{2}$(G10ALLHO3+G10ALLLO3) – G10ALLNO3.

[c] Combined aerosol effects are calculated with the ModelE2-YIBs climate model, e.g., present-day aerosol effect is G10ALLNO3 – G10NATNO3.

[d] Separate aerosol effects are calculated with the offline YIBs vegetation model driven with forcings from the climate model (Table S3).

[e] The net impact of O_3 damages and aerosol effects, for example at present day, is calculated as $\frac{1}{2}$(G10ALLHO3+G10ALLLO3) – G10NATNO3.

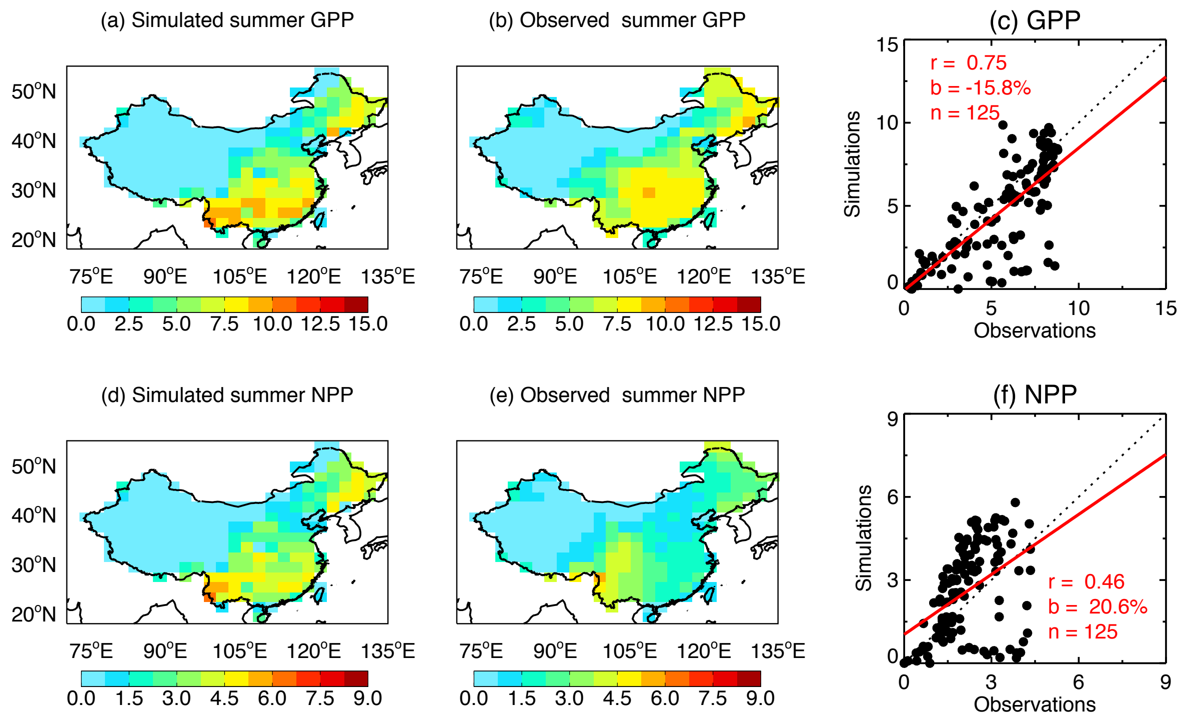

Figure 1. Evaluation of simulated summertime carbon fluxes by ModelE2-YIBs. Panels show GPP (top row) and NPP (bottom row) over China. Simulation results (a, d) are the average of G10ALLHO3 and G10ALLLO3, which are performed with the climate model ModelE2-YIBs using high and low ozone damage sensitivities (Table 2). The correlation coefficients (r), relative biases (b), and number of grid cells (n) for the comparisons are listed on the scatter plots. Units: g C m^{-2} day^{-1}.

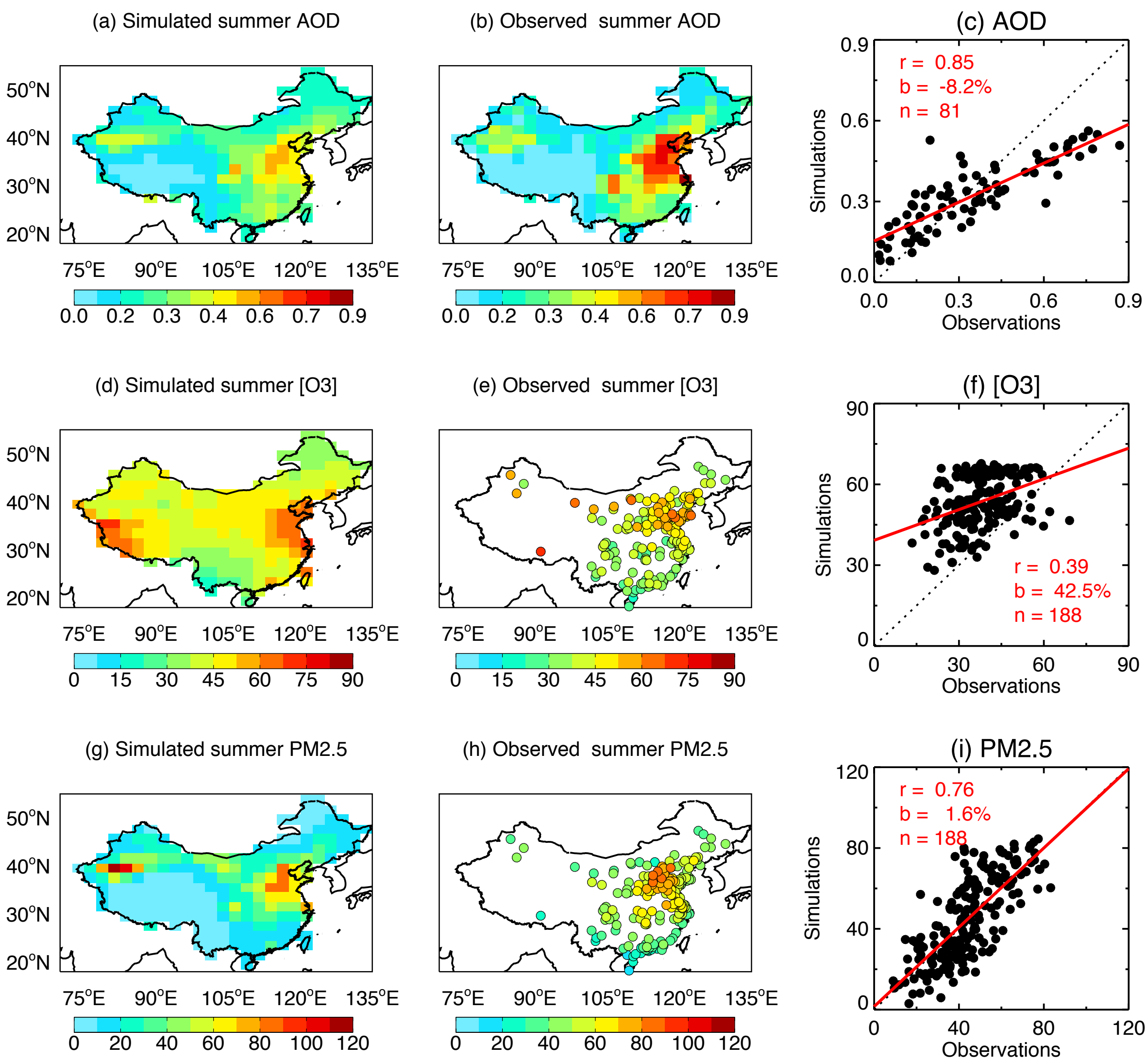

Figure 2. Evaluation of simulated summertime air pollution in China. Evaluations shown include (a) aerosol optical depth (AOD) at 550 nm, (d) [O_3] (units: ppbv), and (g) $PM_{2.5}$ concentrations (units: μg m^{-3}) with observations from (b) the satellite retrieval of the MODIS (averaged for 2008-2012), and (e) and (h) measurements from 188 ground-based sites (at the year 2014). Simulation results are from G10ALLNO3 performed with the climate model ModelE2-YIBs (Table 2). The correlation coefficients (r), relative biases (b), and number of sites/grids (n) for the comparisons are listed on the scatter plots.

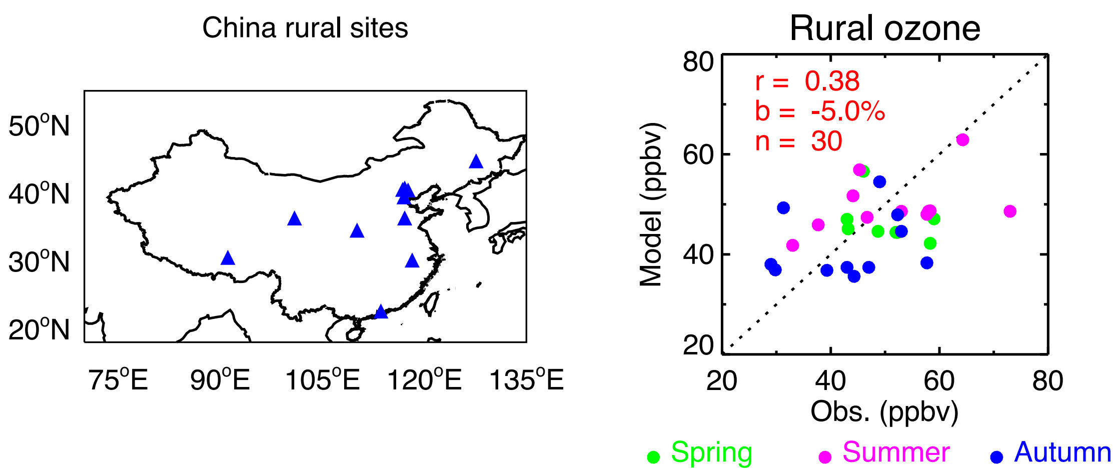

Figure 3. Evaluation of simulated [O_3] at rural sites in China. Simulation results are from G10ALLNO3 performed with the climate model ModelE2-YIBs (Table 2). For the scatter plots, green, pink, and blue points represent values in spring, summer, and autumn, respectively. The data sources of all sites are listed in Table S4.

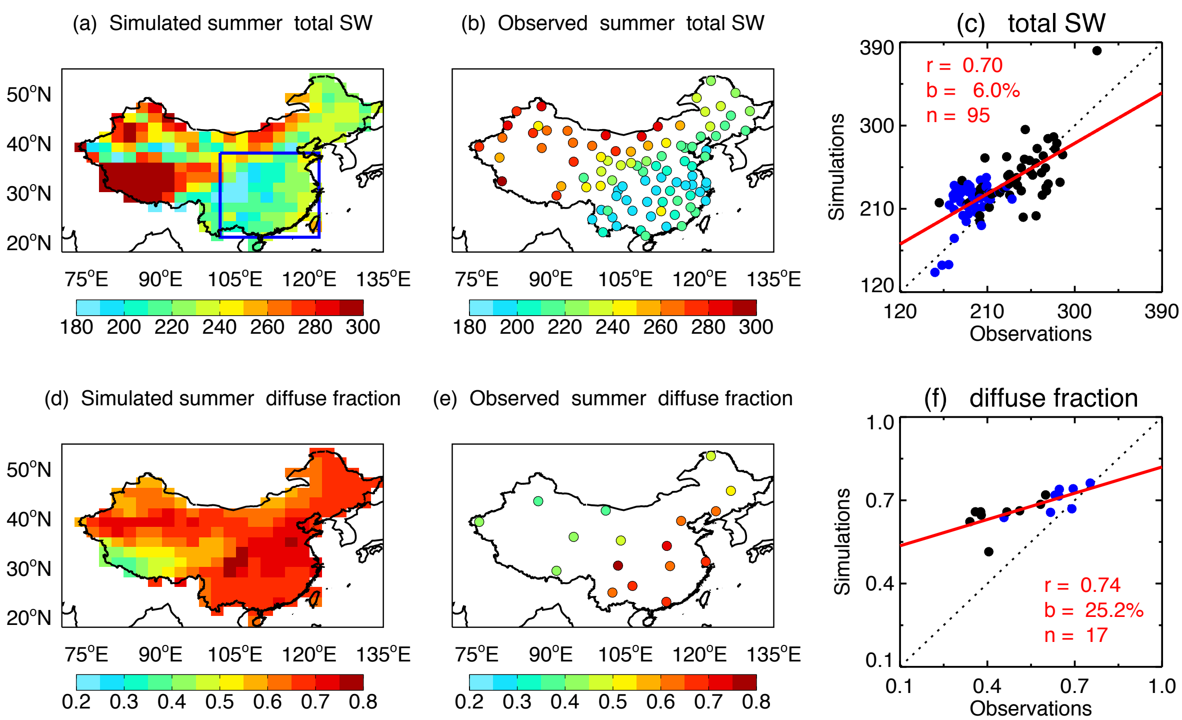

Figure 4. Evaluation of simulated radiation fluxes by ModelE2-YIBs. Panels show summertime surface (a) total shortwave radiation (units: W m^{-2}) and (d) diffuse-to-total fraction with (b, e) observations from 106 sites. Simulation results are from G10ALLNO3 performed with the climate model ModelE2-YIBs (Table 2). The correlation coefficients (r), relative biases (b), and number of sites (n) for the comparisons are listed on the (c, f) scatter plots. The blue points in the scatter plots represent sites located within the box regions in southeastern China as shown in (a).

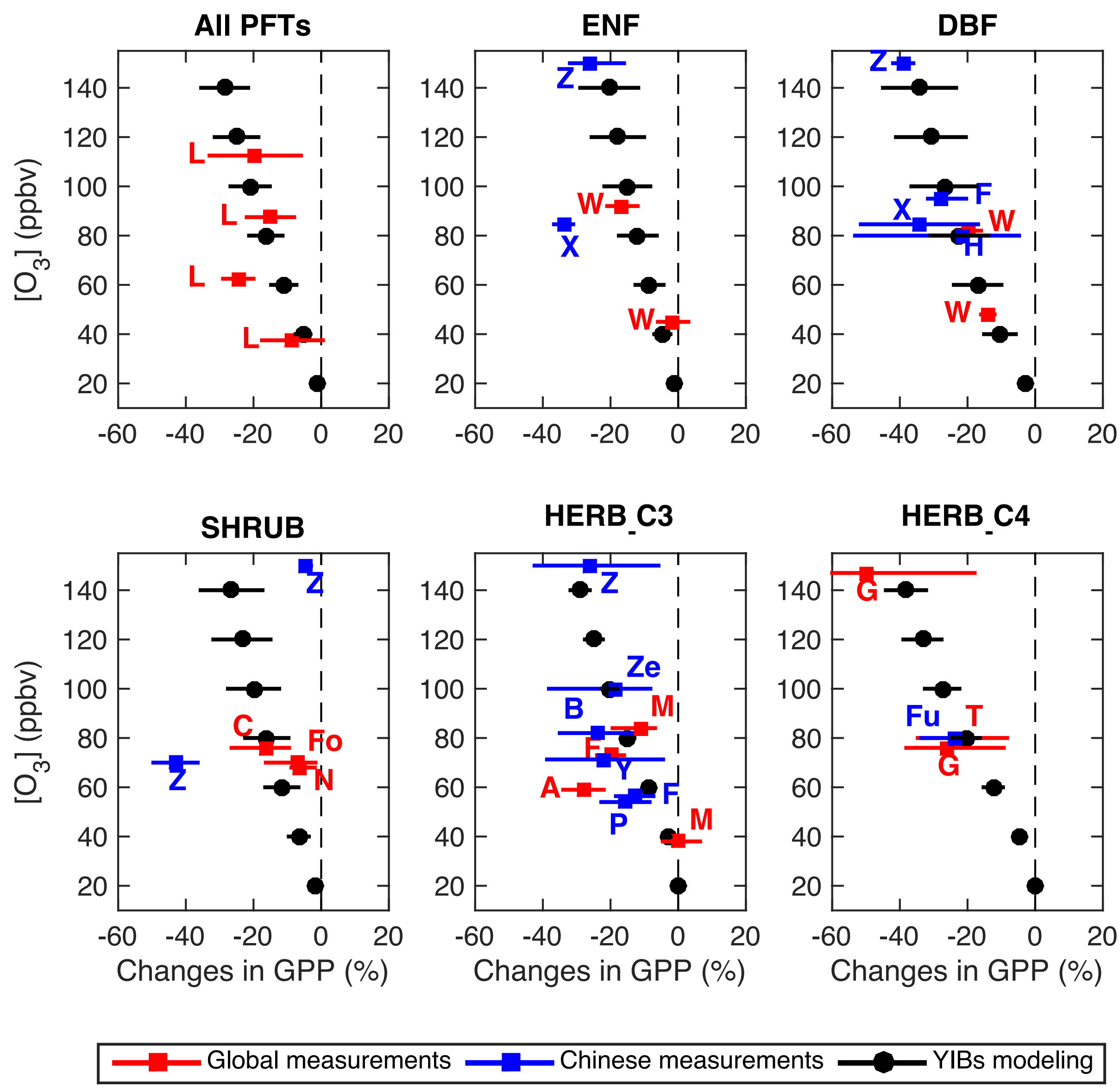

Figure 5. Comparison of predicted changes in summer GPP by O_3 with measurements. Simulations are performed using the offline YIBs vegetation model (Table S2) and averaged for all grid squares over China weighted by the area of a specific PFT. Black points show the simulated mean reductions with error bars indicating damage range from low to high O_3 sensitivity. Solid squares with error bars show the results (mean plus uncertainty) based on measurements reported in the literature (Table S1). Experiments performed for vegetation types in China are denoted with blue symbols. The author initials are indicated for the corresponding studies.

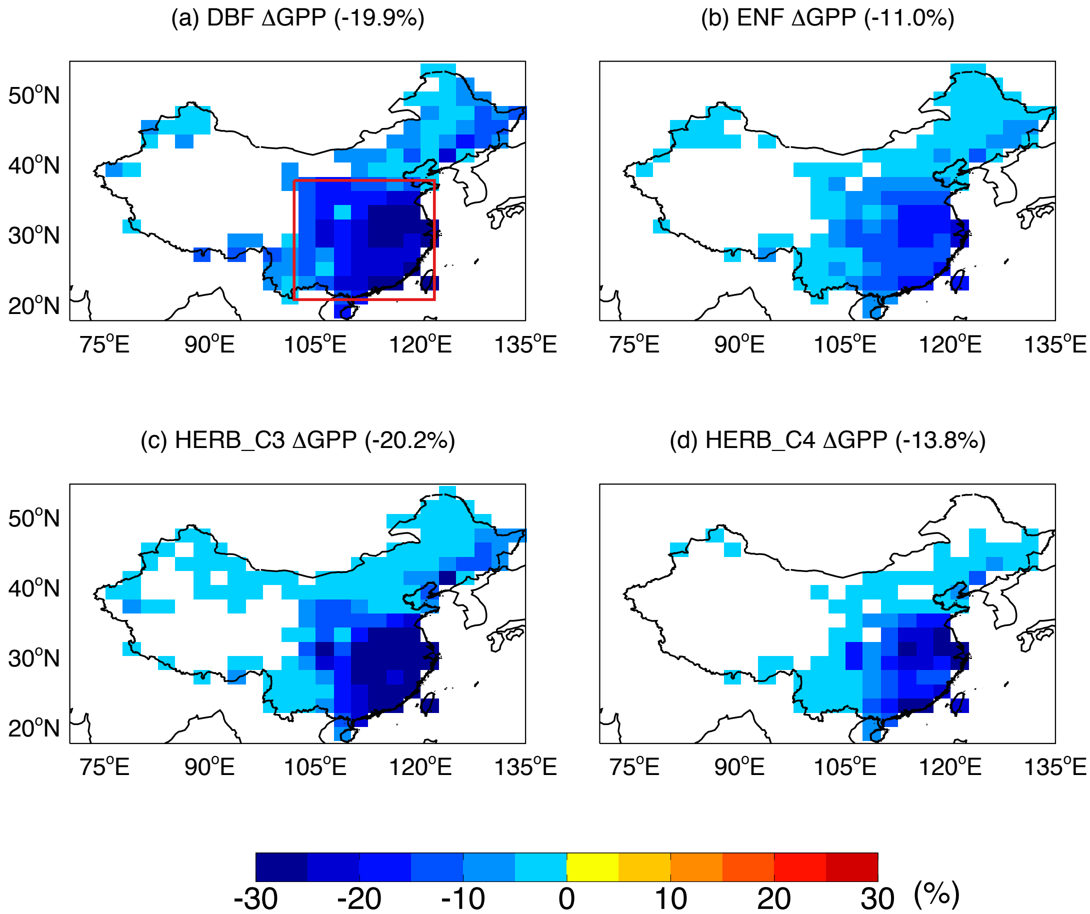

Figure 6. Predicted offline percentage damage to summer GPP caused by O_3. Panels show the damages to (a) ENF (evergreen needleleaf forest), (b) DBF (deciduous broadleaf forest), (c) C3 herbs, and (d) C4 herbs over China in the year 2010. Simulations are performed with the climate model ModelE2-YIBs, which does not feed O_3 vegetation damages back to affect biometeorology, plant growth, and ecosystem physiology. The results are averaged for the low and high damaging sensitivities:

$$\left(\frac{1}{2}(\mathrm{G10ALLHO3\_OFF}+\mathrm{G10ALLLO3\_OFF})/\mathrm{G10ALLNO3}-1\right)\times 100\%$$

The average value over the box domain of (a) is shown in the title bracket of each subpanel.

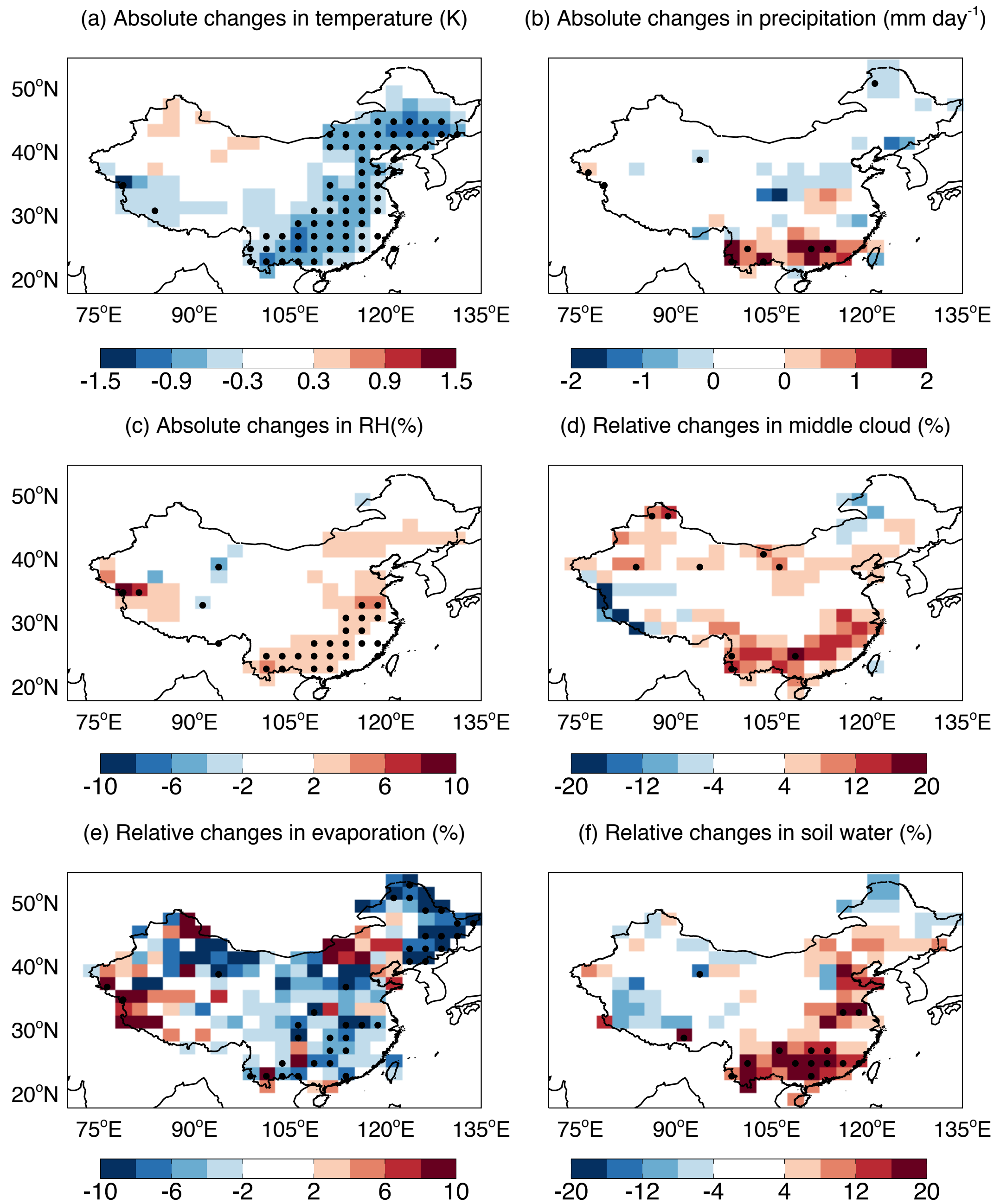

Figure 7. Changes in summer meteorology due to direct radiative effects of anthropogenic aerosols. All changes are calculated as the differences between the simulations G10ALLNO3 and G10NATNO3. For (a) temperature, (b) precipitation, and (c) relative humidity, we show the absolute changes as G10ALLNO3 – G10NATNO3. For (d) middle cloud cover, (e) evaporation, and (f) soil water content, we show the relative changes as (G10ALLNO3/G10NATNO3 – 1) × 100%. Significant changes (p<0.05) are marked with black dots.

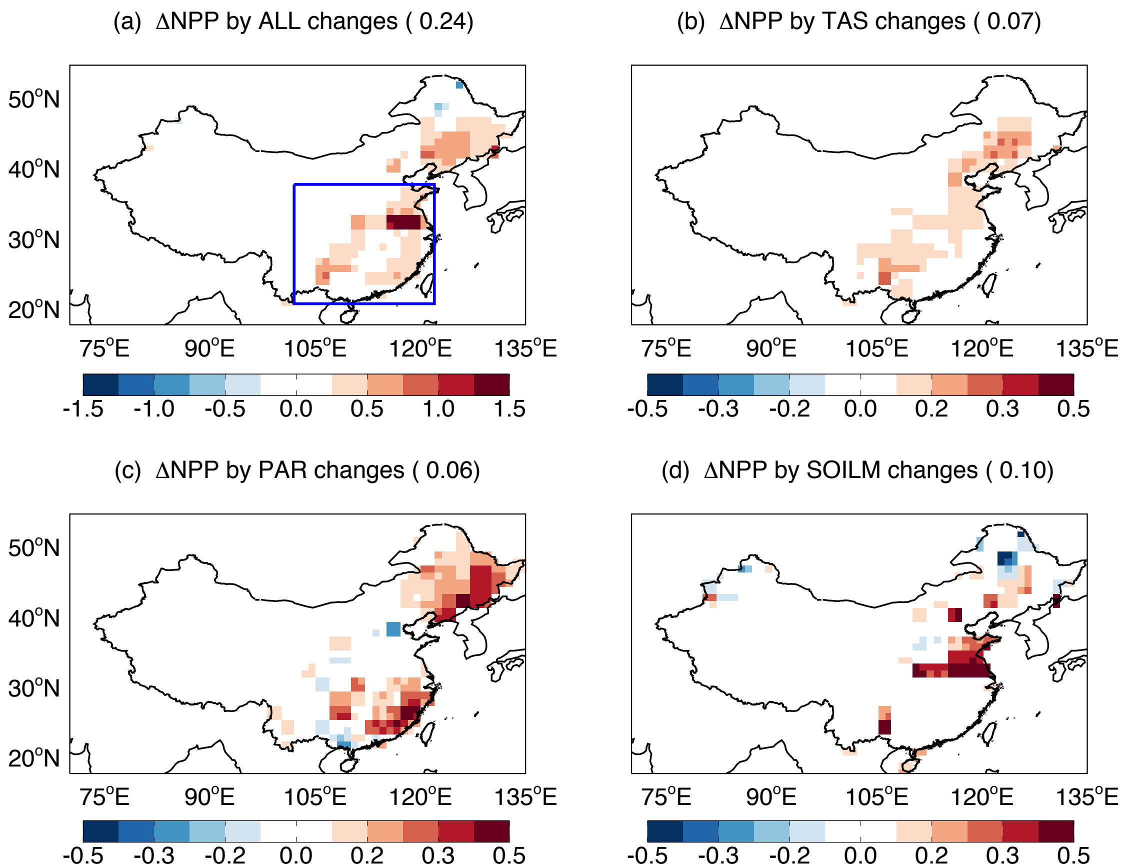

Figure 8. Decomposition of aerosol-induced changes in summer NPP. Changes in NPP are caused by aerosol-induced changes in (b) surface air temperature, (c) photosynthetically active radiation (PAR), (d) soil moisture, and (a) the combination of above three effects. Simulations are performed with the offline YIBs vegetation model driven with meteorological forcings simulated with the ModelE2-YIBs climate model (Table S3). The NPP responses to PAR include the DRF effects. The color scale for the first panel is different from the others. The average NPP perturbation over the box domain in a is shown in the bracket of each title. Units: g C m^{-2} day^{-1}.

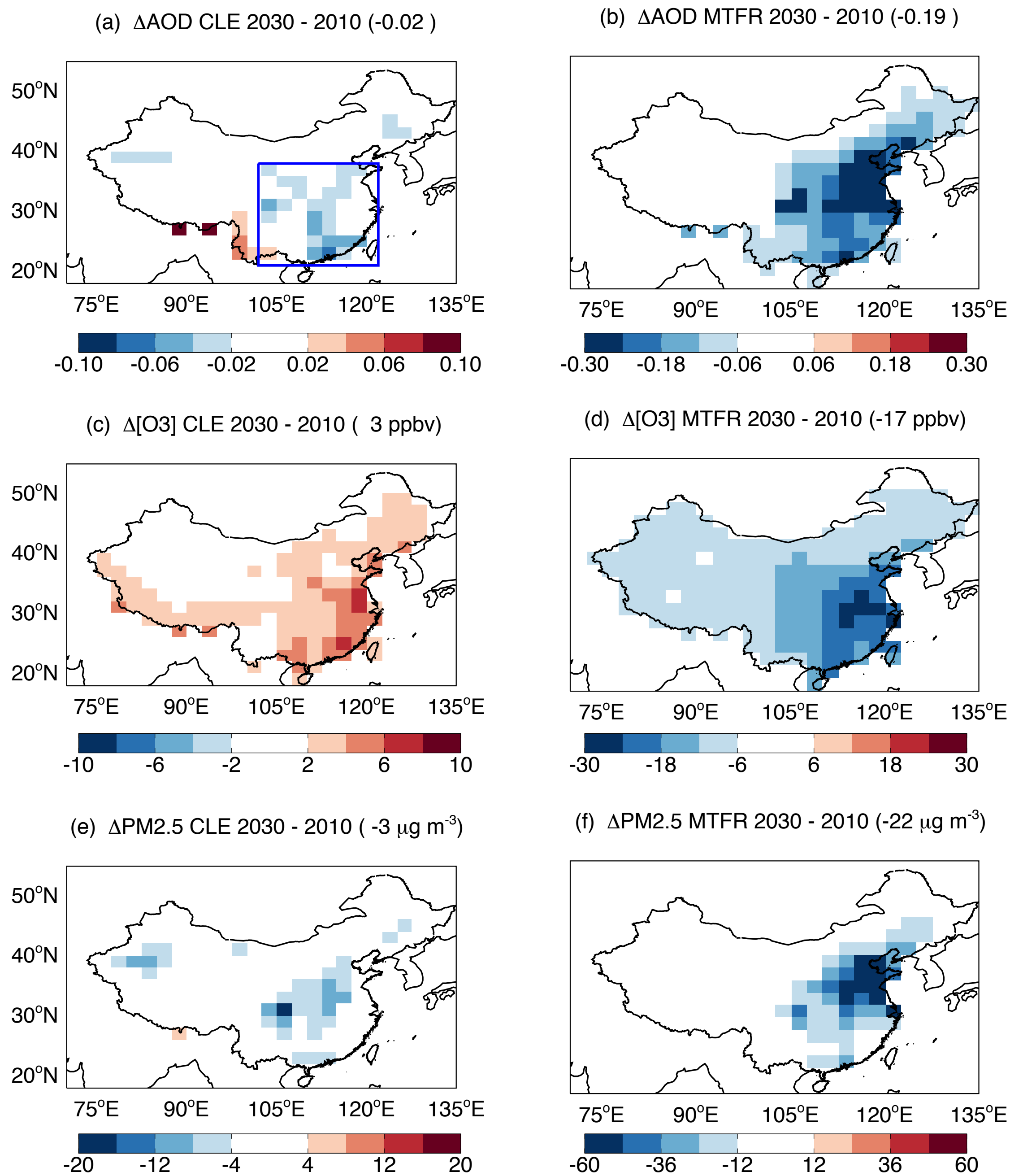

Figure 9. Predicted changes in summertime air pollution by 2030. Panels shown are for (a, b) AOD, (c, d) $[O_3]$, and (e, f) $PM_{2.5}$ concentrations for the year 2030 relative to 2010 based on scenarios of (left) current legislation emissions (CLE) and (right) maximum technically feasible reduction (MTFR). Results for the left panels are calculated as (G30ALLNO3 – G10ALLNO3). Results for the right panels are calculated as (M30ALLNO3 – G10ALLNO3). The average value over the box domain of (a) is shown in the title bracket of each subpanel.

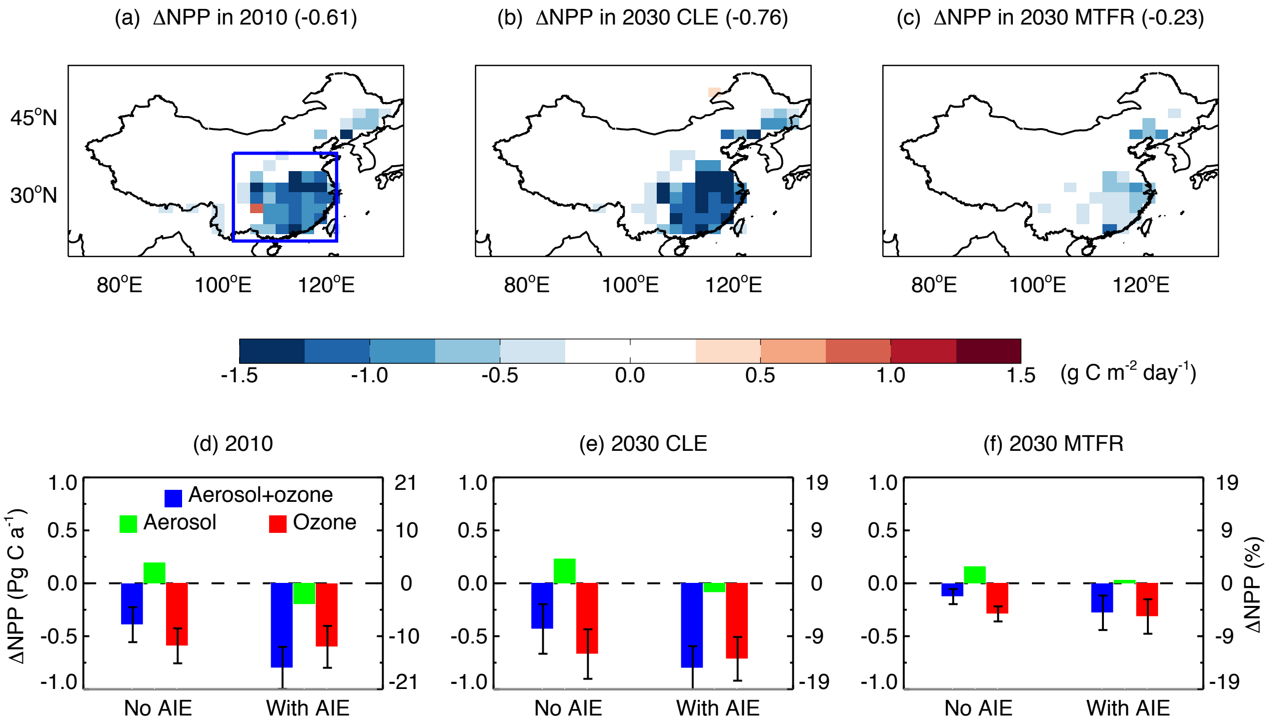

Figure 10. Impacts of air pollution on NPP in the whole of China. Results shown are combined effects of aerosol and O_3 on the summer NPP in (a) 2010, (b) 2030 with CLE scenario, and (c) 2030 with MTFR scenario. Results for the top panels do not include aerosol indirect effects (AIE) but do include the meteorological response to aerosol direct radiative effects. The average NPP perturbation over the box domain in (a) is shown in the bracket of each title. The perturbations to annual total NPP by aerosol, O_3, and their sum over the whole China are shown in (d-f) for different periods, with (right) and without (left) inclusion of AIE. Damages by O_3 are averaged for low and high sensitivities with error bars indicating ranges. The percentage changes are calculated based on NPP without AIE. Simulations are performed with the ModelE2-YIBs model. Only the significant changes ($p < 0.05$) are shown in (a-c).